This article has been accepted for publication in a future issue of this journal, but has not been fully edited. Content may change prior to final publication. Citation information: DOI 10.1109/TCNS.2021.3084444, IEEE Transactions on Control of Network Systems

Singular Perturbation and Small-signal Stability for Inverter Networks

Saber Jafarpour, *Member, IEEE,* Victor Purba, *Student Member, IEEE,* Brian B. Johnson, *Member, IEEE,* Sairaj V. Dhople, *Member, IEEE,* and Francesco Bullo, *Fellow, IEEE*

***Abstract*—This paper examines small-signal stability of electrical networks composed dominantly of three-phase grid-following inverters. We show that the mere existence of a high-voltage power flow solution does not necessarily imply small-signal stability; this motivates us to develop a framework for stability analysis that systematically acknowledges inverter dynamics. We identify a suitable time-scale decomposition for the inverter dynamics, and using singular perturbation theory, obtain an analytic sufficient condition to verify small-signal stability. Compared to the alternative of performing an eigenvalue analysis of the full-order network dynamics, our analytic sufficient condition reduces computational complexity and yields insights on the role of network topology and constitution as well as inverter-filter and control parameters in small-signal stability. Numerical simulations for a radial network validate the approach and illustrate the efficiency of our analytic conditions for designing and monitoring grid-tied inverter networks.**

I. Introduction

Problem description and motivation: The ongoing shift from fossil-fuel-driven synchronous generators to power-electronics-interfaced renewable energy is leading to changes in how power grids are modeled, analyzed, and controlled. While synchronous generators are generally rated at several hundreds of MVA and installed on the transmission backbone, power electronics inverters are distributed across both transmission and distribution subsystems and are generally much smaller in capacity. Furthermore, synchronous generators have large rotating masses that buffer supply-demand fluctuations and limit frequency excursions during transients, whereas inverters have very different dynamics (attributable dominantly to output filters and digital controllers [31]) and they possess no moving parts. Future grids will have large number of power-electronics circuits with highly distributed architecture as inverters assume a more prominent role, and this will necessitate the development of compatible models and computationally efficient stability-analysis approaches.

Most commercial inverters on the market for residential and utility-scale applications are *grid-following*. This means inverters inject currents while synchronized to the voltage at their terminals which is assumed to be set externally by the bulk grid. In effect, grid-following inverters act as voltage-following current sources. In recent years, there has been increased attention on *grid-forming* inverter technology, whereby—much like conventional synchronous generators—terminal voltage and frequency are modulated as a function of real- and reactive-power injections. Indeed, while grid-forming technology may very well be the solution for grids with penetration levels approaching 100%, in the foreseeable future, it is likely that the bulk grid will see conventional synchronous generators co-exist alongside a large number of grid-following inverters. For instance, in Oahu, Hawaii, at least $800,000$ micro-inverters interconnect photovoltaic panels to the grid, producing as much power as the state's largest conventional power plant, Konkar [8]. This motivates the problem of stability analysis for large-scale networks composed dominantly of grid-following inverters that we examine.

The inverter dynamical model that we investigate is composed of a current controller, a power controller, a PLL, and an LCL filter. This is prototypical and mirrors models published widely in the literature [16]–[19], [22], [23], [27]. We propose a framework that leverages singular perturbation methods to obtain an analytic, computationally light-weight condition for small-signal stability assessment of three-phase distribution networks with grid-following inverters. Our solution strategy yields an analytic condition for stability that is agnostic to system size and clearly highlights the role of the network topology and pertinent system parameters on system stability. Due to the complexity of the involved dynamics, most prior art on stability of inverter-based systems has typically focused on simplified models that neglect inner control loops with fast dynamics [25]. Some exceptions are [1], [32], where stability of full-order inverter models are studied in grid-connected networks. However, these studies are restricted to parallel networks of inverters and are not applicable to networks with general topologies. In some cases, detailed inverter models have been considered in general networks, but system stability has only been studied for a single inverter or a small network of inverters using numerical eigenvalue analysis. For instance, small-signal stability is analyzed in the literature using eigenvalue analysis for a single grid-following inverter under unintentional islanding in [28], for the IEEE 37-bus system with 7 inverters in [22], [23], for a radial network consisting of 3 inverters in [17], and for a single-machine-single-inverter network in [13]. The article [15] provides interesting insights about the role of inverter structure in small-signal stability of transmission grids with different levels of penetration of inverters. Using numerical simulations for the IEEE 9-bus system with one grid-following and one grid-forming inverter, this paper reveals the substantial effect of grid-following dynamics in the small-signal stability of inverter networks.

S. Jafarpour and F. Bullo are with the Center of Control, Dynamical Systems and Computation, UC Santa Barbara, CA 93106, USA. E-mail: (saber, bullo@ucsb.edu). V. Purba and S. V. Dhople are with Department of Electrical and Computer Engineering at the University of Minnesota, Minneapolis, MN 55414 USA. E-mail: (purba002, dhople@umn.edu). Brian B. Johnson is with the Department of Electrical Engineering, University of Washington, Seattle, Washington, WA 98195 USA. E-mail: (brianbj@uw.edu)

2325-5870 (c) 2021 IEEE. Personal use is permitted, but republication/redistribution requires IEEE permission. See http://www.ieee.org/publications_standards/publications/rights/index.html for more information.
Authorized licensed use limited to: University of Washington Libraries. Downloaded on April 19,2022 at 20:42:08 UTC from IEEE Xplore. Restrictions apply.

This article has been accepted for publication in a future issue of this journal, but has not been fully edited. Content may change prior to final publication. Citation information: DOI 10.1109/TCNS.2021.3084444, IEEE Transactions on Control of Network Systems

Understandably, while numerical eigenvalue analysis of the linearized network is indeed a reasonable strategy, this approach comes with significant drawbacks. First, the large size of the network combined with the high dimensionality of the inverter model pose computational challenges to analysis. Furthermore, studying small-signal stability by computing eigenvalues of the linearized system does not reveal the role of critical network attributes on system stability, insights, which if formalized appropriately can facilitate analysis.

Several works have also used time-scale separation and singular perturbation to study the qualitative dynamic behaviors of the inverter networks (see, e.g., [23] and the survey [25]). In [25], a generic time-scale approach is used to study stability of inverter networks. However, this approach does not explicitly identify the time-scale parameter and treats all the states of the grid-following inverters as fast variables. In [23], a suitable time-scale decomposition for a class of inverters is identified and iterative scheme for model reduction is proposed.

On a tangential note, it must be acknowledged that there is a growing body of work on stability assessment of synchronous generators and grid-forming inverter systems, and this includes approaches that have applied model-order reduction using singular perturbation analysis. For instance, in [2], [6], [9], [26], [29], model-reduction approaches based on singular perturbation are proposed to study stability and control of grid-forming inverters. In [14], singular perturbation is applied to obtain a hierarchy of reduced-order models for inverters in the grid-forming mode. In [2], a hierarchical time-scale approach is used to estimate the trajectories of networks of grid-forming inverters. In [26], a Lyapunov approach is used to study multiple-time-scale separation in inverter networks modeled as nested interconnected systems. We refer interested readers to [24] for a survey on singular perturbation methods and to [25] for a survey on application of singular perturbation in stability and control of inverters.

Contributions: We make several contributions to the study of small-signal stability of grid-following inverter networks. First, we show that adopting a static model for grid-following inverters (as fixed sources of active and reactive power) and neglecting fast dynamics induced by the inverters' control loops may lead to erroneous conclusions regarding stability (see Example 4). This underscores the importance of acknowledging a full-order model for stability analysis. We start by introducing a model for grid-tied inverter networks that acknowledges line dynamics and where each inverter is modeled using a 13th-order model. Next, we uncover a correspondence between the equilibrium points of the dynamics and the solutions of the algebraic power-flow equations. The main contribution of this paper, i.e., an analytic sufficient condition for small-signal stability, is derived in the context of a dimensionless transcription of the involved models which leads to the identification of a physically insightful parametrization of the inverters. We show that certain assumptions on the range of parameters result in a time-scale decomposition of the system. Using singular perturbation analysis, we propose an analytic sufficient condition which guarantees small-signal stability over a given parametric regime. As a unique contribution, we emphasize that the dimensionless form of the network equations as well as the regularity of the singular perturbation problem (i.e., existence of isolated quasi-steady state manifolds) are critical steps in a rigorous time-scale analysis. Over this specified parametric regime, our analytic sufficient condition can also be interpreted as a lower bound on the stability threshold of the network and allows us to check system stability with minimal computational complexity. Furthermore, in the special case of resistive networks, our sufficient condition reduces to checking Hurwitzness of a Metzler matrix, something that can be implemented efficiently via linear programming (see [21]).

In the literature, small-signal stability of inverter networks is studied using eigenvalue analysis for the full-order models (see, e.g., [15], [17]) or for the reduced-order models (see, e.g., [2], [14], [23]). Compared to performing eigenvalue analysis for the full-order system, our proposed analytically driven sufficient condition reduces computational complexity by addressing the high dimensionality of the underlying dynamics (the inverter model we study has 13 dynamical states) and it demarcates the role of the network (topology and constitution) and pertinent inverter dynamics (filter and controller parameters). Compared to the model-order-reduction approaches in [2], [14], our framework can capture the dynamic stability of networks of grid-following inverters. Moreover, while many existing approaches in the literature only outline iterative schemes for model reduction (see [23]), our analysis provides an explicit reduced-order model. Finally, we provide several case studies to validate the analysis.

Notation: Vectors and matrices. We denote the set of real numbers by $\mathbb{R}$, the set of complex numbers by $\mathbb{C}$, the set of complex numbers with negative real part by $\mathbb{C}_-$, the set of binary n-tuples by $\mathbb{Z}_2^n$, and the n-dimensional torus by $\mathbb{T}^n$. We define $\mathrm{i} = \sqrt{-1}$. We identify the complex plane $\mathbb{C}$ with the real plane $\mathbb{R}^2$. For a complex number $v = v_1 + \mathrm{i}v_2 \in \mathbb{C}$, the norm of v is $|v| = \sqrt{v_1^2 + v_2^2}$ and the argument of v, $\arg(v)$, is the angle between v and the positive imaginary axis. We denote the identity matrix of dimension n by I_n, the n-column vector of zeros with $\mathbb{0}_n$, and the n-column vector of ones with $\mathbb{1}_n$. For a matrix $A = \{a_{ij}\} \in \mathbb{C}^{n\times m}$, we denote the trace by $\mathrm{tr}(A)$, the determinant by $\det(A)$, and ∞-norm by $\|A\|_\infty = \max_i \sum_{j=1}^n |a_{ij}|$. For two real symmetric matrices $A, B \in \mathbb{R}^{n\times n}$ we write $A \succ B$ if $A - B$ is positive definite. A real square matrix $A \in \mathbb{R}^{n\times n}$ is Metzler if all its off-diagonal entries are non-negative. For two square matrices $A \in \mathbb{R}^{n\times n}$ and $B \in \mathbb{R}^{m\times m}$, the tensor product is denoted by $A \otimes B$. For a vector $\mathrm{x} \in \mathbb{C}^n$, we denote $\mathrm{diag}(\mathrm{x})$ by $[\mathrm{x}]$.

From n-complex variables to $2n$-real variables. For every complex $Z = X + \mathrm{i}Y \in \mathbb{C}$, the associated real variable in the real plane is denoted by $z = (x, y)^\top \in \mathbb{R}^2$. We will frequently use matrix $\mathcal{J} = \begin{pmatrix} 0 & -1 \\ 1 & 0 \end{pmatrix}$, matrix $\mathcal{H} = \begin{pmatrix} 0 & 1 \\ 1 & 0 \end{pmatrix}$, and the rotation matrix (parameterized by angle $\theta \in \mathbb{S}^1$) by $\mathcal{R}(\theta) = \begin{pmatrix} \cos(\theta) & \sin(\theta) \\ -\sin(\theta) & \cos(\theta) \end{pmatrix}$. Let $\mathrm{u} \in \mathbb{R}^2$. We define matrix-valued operators $\mathcal{D} : \mathbb{R}^2 \to \mathbb{R}^{2\times 2}$ and $\mathcal{D}' : \mathbb{R}^2 \to \mathbb{R}^{2\times 2}$ by $\mathcal{D}(\mathrm{u}) = \begin{pmatrix} u_1 & u_2 \\ u_2 & -u_1 \end{pmatrix}$ and $\mathcal{D}'(\mathrm{u}) = \begin{pmatrix} u_1 & u_2 \\ -u_2 & u_1 \end{pmatrix}$. All the above matrices and operators can be extended to the n-

2325-5870 (c) 2021 IEEE. Personal use is permitted, but republication/redistribution requires IEEE permission. See http://www.ieee.org/publications_standards/publications/rights/index.html for more information.
Authorized licensed use limited to: University of Washington Libraries. Downloaded on April 19,2022 at 20:42:08 UTC from IEEE Xplore. Restrictions apply.

This article has been accepted for publication in a future issue of this journal, but has not been fully edited. Content may change prior to final publication. Citation information: DOI 10.1109/TCNS.2021.3084444, IEEE Transactions on Control of Network Systems

dimensional complex and $2n$-dimensional real spaces using block diagonal structure. For the brevity of notation, we denote the extended n-dimensional complex ($2n$-dimensional real) matrix/operator with the same symbol as its 1-dimensional complex (2-dimensional real) counterpart. Let $\mathbf{V} \in \mathbb{C}^n$ and $\mathbf{v} \in \mathbb{R}^{2n}$ be the associated real vector, then we define $\|\mathbf{v}\|_{\mathbb{C},\infty} = \|\mathbf{V}\|_\infty$.

Algebraic graph theory. We denote an undirected weighted graph by a triple $G = (\mathcal{N}, \mathcal{E}, A)$, where $\mathcal{N} = \{1, 2, \ldots, n\}$ is the set of nodes and $\mathcal{E} \subseteq \mathcal{N} \times \mathcal{N}$ is the set of edges. The matrix $A = \{a_{ij}\} \in \mathbb{R}^{n\times n}$ is the weighted adjacency matrix. For every node $i \in V$, the degree of the node i is given by $d_i = \sum_{j=1}^n a_{ij}$. For a fixed orientation on G, the incidence matrix of the graph G is denoted by $B \in \mathbb{R}^{n\times m}$. The Laplacian for the graph G is defined by $L = D - A$, where $D = \mathrm{diag}(d_1, d_2, \ldots, d_n)$.

Power systems. We examine balanced AC systems, by which we mean that the three-phase signals have the same amplitude and they are phase shifted by $2\pi/3\,\mathrm{rad}$. We consider two different reference frames. The first is the *global* DQ-frame, and it is a rotating reference frame tied to the nominal grid frequency ω_{nom}. The second, the *local* dq-frame, is with reference to each inverter's terminal voltage vector. For a balanced three-phase signal $x : \mathbb{R}_{\geq 0} \to \mathbb{R}^3$, we denote the dq-frame representation by $x_{\mathrm{dq}} = (x_{\mathrm{d}}, x_{\mathrm{q}})^\top \in \mathbb{R}^2$ and the DQ-frame representation by $x_{\mathrm{DQ}} = (x_{\mathrm{D}}, x_{\mathrm{Q}})^\top \in \mathbb{R}^2$. These are related as follows: $x_{\mathrm{dq}} = \mathcal{R}(\delta)x_{\mathrm{DQ}}$, where $\delta \in \mathbb{S}$ is the angle between the dq-frame and the DQ-frame. We assume that all the electrical signals in the network are balanced [3, Chapter 2]. Therefore, the voltage of the grid is a three-phase AC signal given by the time-varying function $v_{\mathrm{g}}(t) = [v_{\mathrm{ga}}(t), v_{\mathrm{gb}}(t), v_{\mathrm{gc}}(t)]^\top \in \mathbb{R}^3$ and in the global DQ-frame, as $v_{\mathrm{gDQ}} = [0, V_{\mathrm{g}}]^\top$, where V_{g} is the amplitude.

II. Model of Individual Inverter

We briefly overview the dynamics of the type of grid-following 3-phase inverters examined in this work. For a more detailed description of the model, see [19], [22]. The model captures all relevant AC-side dynamics, and is composed of a: i) phase-locked loop (PLL), ii) power controller, iii) current controller, and iv) LC output filter. An illustrative block diagram is given in Fig. 1. The PLL consists of a low-pass filter with cut-off frequency $\omega_{c,\mathrm{PLL}}$, and a PI controller with gains $\mathrm{kp}_{\mathrm{PLL}}$ and $\mathrm{ki}_{\mathrm{PLL}}$. The PLL dynamics are

$$\dot{v}_{\mathrm{PLL}} = \omega_{c,\mathrm{PLL}}(v_{\mathrm{od}} - v_{\mathrm{PLL}}), \tag{1a}$$

$$\dot{\phi}_{\mathrm{PLL}} = -v_{\mathrm{PLL}}, \tag{1b}$$

$$\dot{\delta} = -\mathrm{kp}_{\mathrm{PLL}} v_{\mathrm{PLL}} + \mathrm{ki}_{\mathrm{PLL}}\phi_{\mathrm{PLL}}, \tag{1c}$$

where v_{PLL} and ϕ_{PLL} denote states of the low-pass filter and PI controller, respectively, $\dot{\delta}$ is the output of the PI controller, and v_{od} is the d-component of the output voltage of the inverter. The frequency of the PLL loop is defined by $\omega_{\mathrm{PLL}} = \omega_{\mathrm{nom}} + \dot{\delta}$. The power controller consists of two low-pass filters with cut-off frequency ω_{s} and two PI controllers with gains kp_{s} and ki_{s}. The pertinent dynamics are given by:

$$\dot{s}_{\mathrm{avg}} = \omega_{\mathrm{s}}(s - s_{\mathrm{avg}}), \tag{2a}$$

$$\tilde{i}_{l\mathrm{dq}} = \mathrm{kp}_{\mathrm{s}}\mathcal{H}(s^{\mathrm{ref}} - s_{\mathrm{avg}}) + \mathrm{ki}_{\mathrm{s}}\int \mathcal{H}(s^{\mathrm{ref}} - s_{\mathrm{avg}})dt, \tag{2b}$$

where $s_{\mathrm{avg}} = (p_{\mathrm{avg}}, q_{\mathrm{avg}})^\top \in \mathbb{R}^2$ collects the states of the low-pass filters, $\tilde{i}_{l\mathrm{dq}} \in \mathbb{R}^2$ capture the outputs of the PI controllers (these are the references for the current controller), $s^{\mathrm{ref}} = (p^{\mathrm{ref}}, q^{\mathrm{ref}})^\top \in \mathbb{R}^2$ collects the active- and reactive-power references, and $s = (p, q)^\top \in \mathbb{R}^2$ collects instantaneous active- and reactive-power outputs (measured at the point of common coupling):

$$s = \tfrac{3}{2}\begin{pmatrix} v_{\mathrm{od}}i_{\mathrm{od}} + v_{\mathrm{oq}}i_{\mathrm{oq}} \\ v_{\mathrm{oq}}i_{\mathrm{od}} - v_{\mathrm{od}}i_{\mathrm{oq}} \end{pmatrix} = \tfrac{3}{2}\mathcal{D}(v_{\mathrm{odq}})i_{\mathrm{odq}}.$$

The current controller consists of two PI controllers with gains kp_{c} and ki_{c}, with outputs to be the references for the inverter voltage at the switching terminals v_{idq}:

$$\begin{aligned}\tilde{v}_{\mathrm{idq}} = \mathrm{kp}_{\mathrm{c}}\left(\tilde{i}_{l\mathrm{dq}} - i_{l\mathrm{dq}}\right) + \mathrm{ki}_{\mathrm{c}}\int \left(\tilde{i}_{l\mathrm{dq}} - i_{l\mathrm{dq}}\right)dt \\ + \omega_{\mathrm{PLL}}L_{\mathrm{f}}(\mathcal{J}i_{l\mathrm{dq}}).\end{aligned} \tag{3}$$

Since the switching period is typically much shorter than the filter and controller time constants, we assume that $v_{\mathrm{idq}} = \tilde{v}_{\mathrm{idq}}$. The dynamics of the LC filter (composed of inductance, L_f, and capacitance, C_f) are given by

$$\dot{i}_{l\mathrm{dq}} = \frac{1}{L_{\mathrm{f}}}(v_{\mathrm{idq}} - v_{\mathrm{odq}}) - \omega_{\mathrm{PLL}}(\mathcal{J}i_{l\mathrm{dq}}), \tag{4a}$$

$$\dot{v}_{\mathrm{odq}} = \frac{1}{C_{\mathrm{f}}}(i_{l\mathrm{dq}} - i_{\mathrm{odq}}) - \omega_{\mathrm{PLL}}(\mathcal{J}v_{\mathrm{odq}}), \tag{4b}$$

where $i_{l\mathrm{dq}}$ denotes the inductor current, v_{odq} denotes the capacitor voltage, and i_{odq} denotes the current injected by the inverter into the grid terminals. (See Fig. 1.) Finally, we introduce two new variables $\phi_{\mathrm{s}} := \int(s^{\mathrm{ref}} - s_{\mathrm{avg}})dt$, and $\gamma_{\mathrm{dq}} := \int(\tilde{i}_{l\mathrm{dq}} - i_{l\mathrm{dq}})dt$, that will aid in exposition. The inner- and outer-loop control architecture examined here is ubiquitous, see, e.g., [16]–[19], [22], [23], [27].

Now, we write the dynamical system of the inverters in the global DQ-frame. To this end, we introduce:

$$\gamma_{\mathrm{DQ}} = \mathcal{R}(-\delta)\gamma_{\mathrm{dq}},\ i_{\mathrm{lDQ}} = \mathcal{R}(-\delta)i_{l\mathrm{dq}},\ v_{\mathrm{oDQ}} = \mathcal{R}(-\delta)v_{\mathrm{odq}}.$$

For vector y with time-varying entries, the time derivatives in the global DQ-frame and local dq-frame are related by

$$\dot{y}_{\mathrm{DQ}} - \mathcal{J}\mathcal{R}(-\delta)\dot{\delta}y_{\mathrm{DQ}} = \mathcal{R}(-\delta)\dot{y}_{\mathrm{dq}}.$$

Leveraging this identity, the dynamical model for the grid-following inverter in the DQ-frame can be expressed as:

$$\dot{y} = f(y) + g(y)i_{\mathrm{oDQ}} + Cs^{\mathrm{ref}}, \tag{5}$$

where $y = (v_{\mathrm{PLL}}, \phi_{\mathrm{PLL}}, \delta, \phi_{\mathrm{s}}^\top, s_{\mathrm{avg}}^\top, \gamma_{\mathrm{DQ}}^\top, i_{\mathrm{lDQ}}^\top, v_{\mathrm{oDQ}}^\top)^\top \in \mathbb{R}^{13}$ captures states of the inverter in the global DQ reference frame, $s^{\mathrm{ref}} = (p^{\mathrm{ref}}, q^{\mathrm{ref}})^\top \in \mathbb{R}^2$ captures the references for active and reactive power, $f : \mathbb{R}^{13} \to \mathbb{R}^{13}$ is the drift vector field, and $g : \mathbb{R}^{13} \to \mathbb{R}^{13\times 2}$, and $C \in \mathbb{R}^{13\times 2}$ are control vector fields. The mappings f, g and the matrix C are obtained from the dynamics governing the current controller, the power controller, the PLL, and the LC filter outlined previously. Given the high dimension of the model that these constructs encode, it would be very challenging to write out individual

2325-5870 (c) 2021 IEEE. Personal use is permitted, but republication/redistribution requires IEEE permission. See http://www.ieee.org/publications_standards/publications/rights/index.html for more information.
Authorized licensed use limited to: University of Washington Libraries. Downloaded on April 19,2022 at 20:42:08 UTC from IEEE Xplore. Restrictions apply.

This article has been accepted for publication in a future issue of this journal, but has not been fully edited. Content may change prior to final publication. Citation information: DOI 10.1109/TCNS.2021.3084444, IEEE Transactions on Control of Network Systems

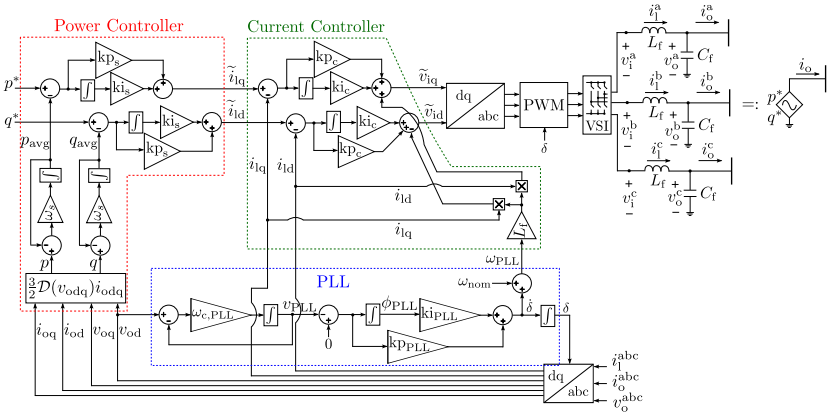

Fig. 1: Block diagram capturing the dynamics of a three phase grid-tied inverter and shorthand representation for the per-phase equivalent circuit. Model includes dynamics arising from the phase locked loop (1), power controller (2), current controller (3), and LC filter (4) [20].

entries explicitly. We ensure that subsequent references to this model are clear in context.

Remark 1. *The model introduced above does not include the DC-side dynamics. This is deliberate; including DC-side dynamics tailored to, e.g., photovoltaic resources and energy-storage devices, would take away from the generality of the results that follow. Another reason that prompts the exclusion relates to the nature of some DC resources. In particular, DC-side dynamics can be neglected if one is interfacing with a resource that presents stiff voltage-source-like behavior or as a result of the application of appropriate fast-acting control loops. It is also worth pointing out that control strategies for DC-side resources, e.g., maximum power point tracking algorithms, cannot always be neatly transcribed into state-space models to facilitate analysis. This last aspect in particular, provides excellent grounds for future work.*

III. Model for Grid-tied Network of Inverters

In this section, we derive the dynamical system model governing the grid-tied network of inverters and loads and study the equilibrium points of the system. We model the network using an undirected, connected, matrix-weighted graph G with node set (buses) $\mathcal{N}$, edge set (branches) $\mathcal{E} \subseteq \mathcal{N} \times \mathcal{N}$, and the symmetric matrix-valued edge weights (admittances) $a_{kj} = a_{jk} = (R_{kj} I_2 + \omega_{\text{nom}} L_{kj} \mathcal{J})^{-1}$, where R_{kj} is the resistance and L_{kj} is the inductance of the line (k, j), for every $(k, j) \in \mathcal{E}$. Suppose B is the incidence matrix of G. There are three types of nodes in the network: we have one *grid bus* with voltage $v_{\text{gDQ}} = [0, V_{\text{g}}]^\top$ denoted by 0. We have $n \geq 1$ *inverter buses* collected in the set $\mathcal{N}_{\text{I}}$, and ℓ *load buses* collected in the set $\mathcal{N}_{\text{L}}$. This setup is well suited for analysis of distribution networks with the stiff voltage source, i.e., the grid bus, modeling the secondary side of the step-down transformer that interfaces the distribution network with the medium-voltage transmission network. The idea here being that the aggregate representation of all transmission-side assets presents itself as a stiff equivalent voltage source. Without loss of generality, we assume that $\mathcal{N}_{\text{L}} = \{1, \dots, \ell\}$ and $\mathcal{N}_{\text{I}} = \{\ell+1, \dots, n+\ell\}$ such that $\mathcal{N} = \{0\} \cup \mathcal{N}_{\text{L}} \cup \mathcal{N}_{\text{I}}$. Therefore $|\mathcal{N}| = 1 + \ell + n$ and we assume that $|\mathcal{E}| = m$. Associated to the matrix-weighted graph, G, we define the nodal admittance matrix by $Y = (B \otimes I_2)\mathcal{A}(B \otimes I_2)^\top \in \mathbb{R}^{2(1+\ell+n)\times 2(1+\ell+n)}$, where $\mathcal{A} \in \mathbb{R}^{2m\times 2m}$ is given by $\mathcal{A} = \text{blkd}(a_{jk})$. The partition $\mathcal{N} = \{0\} \cup \mathcal{N}_{\text{L}} \cup \mathcal{N}_{\text{I}}$ induces the following decomposition of incidence matrix B: $B^\top = \begin{pmatrix} B_0^\top & B_{\text{L}}^\top & B_{\text{I}}^\top \end{pmatrix}$, where $B_0 \in \mathbb{R}^{1\times m}$, $B_{\text{L}} \in \mathbb{R}^{\ell\times m}$, and $B_{\text{I}} \in \mathbb{R}^{n\times m}$, and the following partition for the admittance matrix $Y = \begin{bmatrix} Y_{00} & Y_{0\text{L}} & Y_{0\text{I}} \\ Y_{\text{L}0} & Y_{\text{LL}} & Y_{\text{LI}} \\ Y_{\text{I}0} & Y_{\text{IL}} & Y_{\text{II}} \end{bmatrix}$. For a given variable (parameter) y corresponding to the inverter, we define vector $\mathbf{y} = (y_1^\top, \dots, y_n^\top)^\top$, where y_k is the associated variable (parameter) for the kth inverter.

Inverter model: Using (5), the governing dynamics for *all* inverters in the network can be expressed as:

$$\dot{\mathbf{y}} = F(\mathbf{y}) + G(\mathbf{y})\mathrm{i}_{\text{oDQ}} + C\mathbf{s}^{\text{ref}}, \tag{6}$$

where, in $\mathbf{y} = (y_1^\top, \dots, y_n^\top)^\top \in \mathbb{R}^{13n}$, y_k captures all the dynamic states for the kth inverter, $F(\mathbf{y}) = (f_1^\top(y_1), \dots, f_n^\top(y_n))^\top$, $G(\mathbf{y}) = \text{diag}\,(g_1(y_1), \dots, g_n(y_n))$, and $C = \text{diag}\,(C_1, \dots, C_n)$, where f_k is the drift vector field and g_k and C_k are control vector fields of inverter k.

Load and line models: Let $v_k \in \mathbb{R}^2$ be the kth load voltage (in the DQ-frame) and $i_k \in \mathbb{R}^2$ be the current demand (in the DQ-frame) of the kth load. We collect the nodal voltages and current demands for the loads in $\mathbf{v}_{\text{L}} = (v_1^\top, \dots, v_\ell^\top)^\top \in \mathbb{R}^{2\ell}$ and $\mathbf{i}_{\text{L}} = (i_1^\top, \dots, i_\ell^\top)^\top \in \mathbb{R}^{2\ell}$, respectively. We assume loads are purely resistive; suppose $\mathbf{R}_{\text{L}} \in \mathbb{R}^\ell$ is the vector of load resistances, then we get

$$\mathbf{v}_{\text{L}} = \big(-[\mathbf{R}_{\text{L}}] \otimes I_2\big)\mathbf{i}_{\text{L}}. \tag{7}$$

One could introduce inductive and capacitive elements in the load model, or indeed, consider more detailed dynamic load models, but the added complexity would significantly stretch the notation and distract from the underlying theme and message of the main results. That said, the setup we examine is well suited to networks with a high penetration of inverters where a majority of loads and sources are all interfaced through inverters.

Suppose that the vector of line resistances and line inductances are denoted by $\mathbf{R}_{\mathcal{E}} \in \mathbb{R}^m$ and $\mathbf{L}_{\mathcal{E}} \in \mathbb{R}^m$, respectively; the nodal current injections by $\mathbf{i} = (\mathrm{i}_{\text{g}}^\top, -\mathbf{i}_{\text{L}}^\top, \mathbf{i}_{\text{oDQ}}^\top)^\top$ and nodal voltages by $\mathbf{v} = (v_{\text{gDQ}}^\top, \mathbf{v}_{\text{L}}^\top, \mathbf{v}_{\text{oDQ}}^\top)^\top$. The governing dynamics for the transmission lines are [25, Equation 4.10]:

2325-5870 (c) 2021 IEEE. Personal use is permitted, but republication/redistribution requires IEEE permission. See http://www.ieee.org/publications_standards/publications/rights/index.html for more information.
Authorized licensed use limited to: University of Washington Libraries. Downloaded on April 19,2022 at 20:42:08 UTC from IEEE Xplore. Restrictions apply.

This article has been accepted for publication in a future issue of this journal, but has not been fully edited. Content may change prior to final publication. Citation information: DOI 10.1109/TCNS.2021.3084444, IEEE Transactions on Control of Network Systems

$$([\mathbf{L}_{\mathcal{E}}]\otimes I_2)\dot{\xi}_{\rm DQ} = \big(-[\mathbf{R}_{\mathcal{E}}]\otimes I_2 - \omega_{\rm nom}[\mathbf{L}_{\mathcal{E}}]\otimes\mathcal{J}\big)\xi_{\rm DQ} + (B^\top\otimes I_2)\mathbf{v}, \quad (8)$$

where $\xi_{\rm DQ}\in\mathbb{R}^{2m}$ is the vector of current flows in the lines. Thus we have $\mathbf{i} = (B\otimes I_2)\xi_{\rm DQ}$.

A. Network Model and Dimensionless Transcription

From (6)–(8), the *grid-tied inverter-network dynamics* are:

$$\begin{aligned}\dot{\mathbf{y}} &= F(\mathbf{y}) + G(\mathbf{y})(B_{\rm I}\otimes I_2)\xi_{\rm DQ} + C\mathbf{s}^{\rm ref},\\ ([\mathbf{L}_{\mathcal{E}}]\otimes I_2)\dot{\xi}_{\rm DQ} &= \big(-[\mathbf{R}_{\mathcal{E}}]\otimes I_2 - \omega_{\rm nom}[\mathbf{L}_{\mathcal{E}}]\otimes\mathcal{J}\big)\xi_{\rm DQ} + (B^\top\otimes I_2)\mathbf{v},\end{aligned} \quad (9)$$

where $\mathbf{v} = (v_{\rm gDQ}^\top, \mathbf{v}_{\rm L}^\top, \mathbf{v}_{\rm oDQ}^\top)^\top$ and $\mathbf{v}_{\rm L} = \big(-B_{\rm L}[\mathbf{R}_{\rm L}]\otimes I_2\big)\xi_{\rm DQ}$. We transcribe the differential equations (9) in a dimensionless format. We assume that $s_{\rm nom}$ is the nominal power generation/consumption in the network. For each inverter, we introduce the following dimensionless variables:

$$\widehat{v}_{\rm PLL} := \frac{v_{\rm PLL}}{V_{\rm g}},\quad \widehat{\phi}_{\rm PLL} := \frac{{\rm ki}_{\rm PLL}}{V_{\rm g}{\rm kp}_{\rm PLL}}\phi_{\rm PLL},\quad \widehat{s}_{\rm avg} := \frac{s_{\rm avg}}{s_{\rm nom}},$$
$$\widehat{\phi}_{\rm s} := \frac{V_{\rm g}{\rm ki}_{\rm s}\phi_{\rm s}}{s_{\rm nom}},\quad \widehat{s}^{\rm ref} := \frac{s^{\rm ref}}{s_{\rm nom}},\quad \widehat{\gamma}_{\rm DQ} := \frac{{\rm ki}_{\rm c}\gamma_{\rm DQ}}{V_{\rm g}},\quad \widehat{i}_{\rm lDQ} := \frac{V_{\rm g}i_{\rm lDQ}}{s_{\rm nom}}.$$

For the network, we introduce the dimensionless parameters

$$\widehat{\xi}_{\rm DQ} := V_{\rm g}s_{\rm nom}^{-1}\xi_{\rm DQ},\quad \widehat{\mathbf{v}} := V_{\rm g}^{-1}\mathbf{v},\quad \widehat{\mathbf{i}} := V_{\rm g}s_{\rm nom}^{-1}\mathbf{i}.$$

While the above scaling may be reminiscent of the classical per-unit representation frequently employed in power-system analysis, there are several notable points of departure. In particular, the classical per-unit representation is typically only utilized to scale impedances, currents, voltages, and power values for steady-state analysis of power networks leveraging phasors. In contrast, we utilize the dimensionless transcription for scaling *time-domain* signals beyond *physical-layer* electrical quantities (referenced above) to also include, e.g., *controller states*.

We also isolate time-constants of different sub-systems:

- for the PLL low-pass filter: $\tau_{\rm PLL} = \omega_{\rm c,PLL}^{-1}$, $\tau'_{\rm PLL} = (V_{\rm g}{\rm kp}_{\rm PLL})^{-1}$;
- for the PLL PI controller: ${\rm T}_{\rm PLL} = \frac{{\rm kp}_{\rm PLL}}{{\rm ki}_{\rm PLL}}$;
- for the low-pass filter of the power controller: $\tau_{\rm s} = \omega_{\rm s}^{-1}$;
- for tracking in the power controller: $\tau'_{\rm s} = (V_{\rm g}{\rm ki}_{\rm s})^{-1}$;
- for the PI controller in the power controller: ${\rm T}_{\rm s} = \frac{{\rm kp}_{\rm s}}{{\rm ki}_{\rm s}}$;
- for the current controller: $\tau_{\rm c} = V_{\rm g}^2({\rm ki}_{\rm c}s_{\rm nom})^{-1}$;
- for the PI controller in the current controller: ${\rm T}_{\rm c} = \frac{{\rm kp}_{\rm c}}{{\rm ki}_{\rm c}}$;
- for the LC filter: $\tau_{\rm LC} = \frac{{\rm L_f}}{\sqrt{\omega_{\rm nom}^{-2}{\rm C}_{\rm f}^{-2}+\omega_{\rm nom}^2{\rm L}_{\rm f}^2}}$ and $\tau'_{\rm LC} = \frac{{\rm C_f}}{\sqrt{\omega_{\rm nom}^2{\rm C}_{\rm f}^2+\omega_{\rm nom}^{-2}{\rm L}_{\rm f}^{-2}}}$ and $\tau''_{\rm LC} = {\rm C_f}\omega_{\rm nom}s_{\rm nom}^{-1}V_{\rm g}^2$;
- for line $e\in\mathcal{E}$ in the network: $\tau_{\rm e} = \frac{L_e}{\sqrt{R_e^2+\omega_{\rm nom}^2L_e^2}}$ and $\tau'_{\rm e} = s_{\rm nom}V_{\rm g}^{-2}\sqrt{R_e^2+\omega_{\rm nom}^2L_e^2}$.

With these preliminaries in place, the *dimensionless grid-tied inverter-network dynamics* can be expressed as:

$$\dot{\widehat{\mathbf{v}}}_{\rm PLL} = [\boldsymbol{\tau}_{\rm PLL}]^{-1}(\widehat{\mathbf{v}}_{\rm od} - \widehat{\mathbf{v}}_{\rm PLL}), \quad (10a)$$
$$\dot{\widehat{\phi}}_{\rm PLL} = -[\mathbf{T}_{\rm PLL}]^{-1}\widehat{\mathbf{v}}_{\rm PLL}, \quad (10b)$$
$$\dot{\boldsymbol{\delta}} = [\boldsymbol{\tau}'_{\rm PLL}]^{-1}\left(\widehat{\phi}_{\rm PLL} - \widehat{\mathbf{v}}_{\rm PLL}\right), \quad (10c)$$
$$\dot{\widehat{\mathbf{s}}}_{\rm avg} = [\boldsymbol{\tau}_{\rm s}\otimes I_2]^{-1}(\widehat{\mathbf{s}} - \widehat{\mathbf{s}}_{\rm avg}), \quad (10d)$$
$$\dot{\widehat{\boldsymbol{\phi}}}_{\rm s} = [\boldsymbol{\tau}'_{\rm s}\otimes I_2]^{-1}(\widehat{\mathbf{s}}^{\rm ref} - \widehat{\mathbf{s}}_{\rm avg}), \quad (10e)$$
$$\dot{\widehat{\boldsymbol{\gamma}}}_{\rm DQ} = [\boldsymbol{\tau}_{\rm c}\otimes I_2]^{-1}\left(\widetilde{\mathbf{i}}_{\rm lDQ} - \widehat{\mathbf{i}}_{\rm lDQ}\right) + \mathcal{J}[\dot{\boldsymbol{\delta}}]\widehat{\boldsymbol{\gamma}}_{\rm DQ}, \quad (10f)$$
$$\dot{\widehat{\mathbf{i}}}_{\rm lDQ} = ([\boldsymbol{\tau}_{\rm LC}]^{-1}[\mathcal{X}]\otimes I_2)\,(\widehat{\mathbf{v}}_{\rm lDQ} - \widehat{\mathbf{v}}_{\rm oDQ}) + \mathcal{J}[\dot{\boldsymbol{\delta}}]\widehat{\mathbf{i}}_{\rm lDQ}, \quad (10g)$$
$$\dot{\widehat{\mathbf{v}}}_{\rm oDQ} = ([\boldsymbol{\tau}'_{\rm LC}][\mathcal{X}]\otimes I_2)^{-1}\big(\widehat{\mathbf{i}}_{\rm lDQ} - \widehat{\mathbf{i}}_{\rm oDQ} - [\boldsymbol{\tau}''_{\rm LC}\otimes I_2]\mathcal{J}\widehat{\mathbf{v}}_{\rm oDQ}\big), \quad (10h)$$
$$\dot{\widehat{\xi}}_{\rm DQ} = \big([\boldsymbol{\tau}_{\mathcal{E}}][\boldsymbol{\tau}'_{\mathcal{E}}]\otimes I_2\big)^{-1}\big((B^\top\otimes I_2)\widehat{\mathbf{v}} - \mathcal{Z}\widehat{\xi}_{\rm DQ}\big). \quad (10i)$$

Above,

$$\begin{aligned}\widetilde{\mathbf{i}}_{\rm lDQ} &= [\mathbf{T}_{\rm s}\otimes I_2]\mathcal{R}(-\boldsymbol{\delta})\mathcal{H}\dot{\widehat{\boldsymbol{\phi}}}_{\rm s} + \mathcal{R}(-\boldsymbol{\delta})\mathcal{H}\dot{\widehat{\boldsymbol{\phi}}}_{\rm s},\\ \widehat{\mathbf{v}}_{\rm lDQ} &= [\mathbf{T}_{\rm c}\otimes I_2]\dot{\widehat{\boldsymbol{\gamma}}}_{\rm DQ} + \widehat{\boldsymbol{\gamma}}_{\rm DQ},\\ \widehat{\mathbf{i}} &= (B\otimes I_2)\widehat{\xi}_{\rm DQ},\\ \mathcal{Z} &= [\omega_{\rm nom}\mathbf{L}_{\mathcal{E}}]^{-1}[\mathbf{R}_{\mathcal{E}}]\otimes I_2 + (I_m\otimes\mathcal{J}),\\ \mathcal{X} &= s_{\rm nom}^{-1}V_{\rm g}^2[\omega_{\rm nom}^{-2}\mathbf{C}_{\rm f}^{-2} + \omega_{\rm nom}^2\mathbf{L}_{\rm f}^2]^{\frac{1}{2}},\\ \widehat{\mathbf{v}} &= (\widehat{v}_{\rm gDQ}, \widehat{\mathbf{v}}_{\rm L}, \widehat{\mathbf{v}}_{\rm oDQ})^\top.\end{aligned}$$

The dimensionless grid-tied inverter network dynamics (10a)–(10i) is $(13n+2m)$-dimensional. We denote the state of the dimensionless grid-tied inverter network by $\widehat{\mathbf{x}} = [\widehat{\mathbf{v}}_{\rm PLL}, \widehat{\phi}_{\rm PLL}, \ldots, \widehat{\xi}_{\rm DQ}]^\top\in\mathbb{R}^{13n+2m}$. Our first goal is to find the equilibrium points of the dynamical systems (10a)–(10i).

B. Equilibrium points of the Dimensionless Dynamics

We start by introducing some notation. Let $Y\in\mathbb{R}^{(2n+2)}$ be the admittance matrix of the network. Then

$$\begin{aligned}Y_{\rm red} &:= Y_{\rm II} - Y_{\rm IL}\left(Y_{\rm LL} + [\mathbf{R}_{\rm L}]^{-1}\otimes I_2\right)^{-1}Y_{\rm LI},\\ Y_{\rm C,red} &:= Y_{\rm red} + \omega_{\rm nom}\left([\mathbf{C}_{\rm f}]\otimes J\right),\\ Y_{\rm g} &:= Y_{\rm I0} - Y_{\rm IL}\left(Y_{\rm LL} + [\mathbf{R}_{\rm L}]^{-1}\otimes I_2\right)^{-1}Y_{\rm L0},\\ \mathbf{w} &:= -Y_{\rm red}^{-1}Y_{0\rm g}v_{\rm gDQ},\end{aligned} \quad (11)$$

and the dimensionless parameters $\widehat{Y}_{(\cdot)} := V_{\rm g}^2{\rm s}_{\rm nom}^{-1}Y_{(\cdot)}$ and $\widehat{\mathbf{w}} := -V_{\rm g}{\rm s}_{\rm nom}^{-1}\mathbf{w}$ and $\mathcal{Z}_{\rm L} = \mathcal{Z} + \big([\omega_{\rm nom}\mathbf{L}_{\mathcal{E}}]^{-1}B_{\rm L}^\top[\mathbf{R}_{\rm L}]B_{\rm L}\big)\otimes I_2$. We show that the equilibrium points of the dimensionless grid-tied inverter network dynamics (10) are in correspondence with the solutions of the following power-flow equations:

$$\widehat{\mathbf{s}}^{\rm ref} = \tfrac{3}{2}\mathcal{D}(\widehat{\mathbf{v}}_{\rm oDQ})\widehat{\mathbf{i}}_{\rm oDQ}, \quad (12)$$
$$\widehat{\mathbf{i}}_{\rm oDQ} = \widehat{Y}_{\rm red}\widehat{\mathbf{v}}_{\rm oDQ} + \widehat{Y}_{\rm g}\widehat{v}_{\rm gDQ}. \quad (13)$$

Lemma 2. *For a given reference-power injection $\widehat{s}^{\rm ref}$ to the inverters, the following statements are equivalent:*

(i) $((\widehat{\mathbf{v}}_{\rm oDQ}^{\rm ref})^\top, (\widehat{\mathbf{i}}_{\rm oDQ}^{\rm ref})^\top)^\top\in\mathbb{R}^{4n}$ is a solution for the power-flow equations (12) and (13);

(ii) for every $\alpha = (\alpha_1,\ldots,\alpha_n)^\top\in\mathbb{Z}_2^n$, $\widehat{\mathbf{x}}_\alpha^{\rm ref}\in\mathbb{R}^{13n+2m}$ is an equilibrium point of the dimensionless grid-tied inverter-network dynamics (10) given by

$$\widehat{\mathbf{x}}_\alpha^{\rm ref} = (\mathbb{0}_{2n}, \boldsymbol{\delta}^{\rm ref} + \alpha\pi, (-1)^\alpha\widehat{\phi}_{\rm s}^{\rm ref}, \widehat{\mathbf{s}}^{\rm ref}, \widehat{\boldsymbol{\gamma}}_{\rm DQ}^{\rm ref}, \widehat{\mathbf{i}}_{\rm lDQ}^{\rm ref}, \widehat{\mathbf{v}}_{\rm oDQ}^{\rm ref}, \widehat{\xi}_{\rm DQ}^{\rm ref})^\top$$

with

$$\boldsymbol{\delta}^{\rm ref} = -\arg(\widehat{\mathbf{v}}_{\rm oDQ}^{\rm ref}),\quad \widehat{\mathbf{i}}_{\rm lDQ}^{\rm ref} = [\boldsymbol{\tau}''_{\rm LC}\otimes I_2]\mathcal{J}\widehat{\mathbf{v}}_{\rm oDQ}^{\rm ref} + \widehat{\mathbf{i}}_{\rm oDQ}^{\rm ref},$$
$$\widehat{\phi}_{\rm s}^{\rm ref} = \mathcal{H}\mathcal{R}(\boldsymbol{\delta}^{\rm ref})\widehat{\mathbf{i}}_{\rm lDQ}^{\rm ref},\quad \widehat{\boldsymbol{\gamma}}_{\rm DQ}^{\rm ref} = \widehat{\mathbf{v}}_{\rm oDQ}^{\rm ref},$$

2325-5870 (c) 2021 IEEE. Personal use is permitted, but republication/redistribution requires IEEE permission. See http://www.ieee.org/publications_standards/publications/rights/index.html for more information.
Authorized licensed use limited to: University of Washington Libraries. Downloaded on April 19,2022 at 20:42:08 UTC from IEEE Xplore. Restrictions apply.

This article has been accepted for publication in a future issue of this journal, but has not been fully edited. Content may change prior to final publication. Citation information: DOI 10.1109/TCNS.2021.3084444, IEEE Transactions on Control of Network Systems

$$\widehat{\xi}^{\mathrm{ref}}_{\mathrm{DQ}} = \mathcal{Z}_{\mathrm{L}}^{-1}\big((B_{\mathrm{I}}^{\top}\otimes I_2)\widehat{\mathbf{v}}^{\mathrm{ref}}_{\mathrm{oDQ}} + (B_0^{\top}\otimes I_2)\widehat{v}_{\mathrm{gDQ}}\big).$$

Proof. Regarding $(ii) \implies (i)$, from the power-controllers' dynamics in (10), we can conclude that if $\widehat{\mathbf{x}}^{\mathrm{ref}}_{\alpha}$ is an equilibrium point, then we have $\widehat{\mathbf{s}} = \widehat{\mathbf{s}}^{\mathrm{ref}}$. This implies $\widehat{\mathbf{v}}^{\mathrm{ref}}_{\mathrm{oDQ}}$ and $\widehat{\mathbf{i}}^{\mathrm{ref}}_{\mathrm{oDQ}}$ satisfy (12). Moreover, at the equilibrium point $\widehat{\mathbf{x}}^{\mathrm{ref}}_{\alpha}$, the line dynamics (10i) will simplify to $\widehat{\mathbf{i}}^{\mathrm{ref}} = \widehat{Y}\widehat{\mathbf{v}}^{\mathrm{ref}}$. Using Kron reduction [7], this implies that $\widehat{\mathbf{v}}^{\mathrm{ref}}_{\mathrm{oDQ}}$ and $\widehat{\mathbf{i}}^{\mathrm{ref}}_{\mathrm{oDQ}}$ satisfy (13).

Regarding $(i) \implies (ii)$, suppose $((\widehat{\mathbf{v}}^{\mathrm{ref}}_{\mathrm{oDQ}})^{\top}, (\widehat{\mathbf{i}}^{\mathrm{ref}}_{\mathrm{oDQ}})^{\top})^{\top}$ is a solution to the power flow equations (12) and (13). Then from the PLL dynamics in (10), we have $\widehat{\mathbf{v}}_{\mathrm{PLL}} = \mathbb{0}_n$ and $\widehat{\mathbf{v}}_{\mathrm{od}} = \mathbb{0}_n$. Note that, $\widehat{\mathbf{v}}_{\mathrm{od}} = \mathbb{0}_n$ can be written in the trigonometric form

$$v_{\mathrm{oD}}^{k,\mathrm{ref}}\cos(\delta^{k,\mathrm{ref}}) + v_{\mathrm{oQ}}^{k,\mathrm{ref}}\sin(\delta^{k,\mathrm{ref}}) = 0.$$

This implies that, for every $k \in \{1,\dots,n\}$, there exists $\alpha_k \in \mathbb{Z}_2$ such that $\delta^{k,\mathrm{ref}} = -\arg(v_{\mathrm{oDQ}}^{k,\mathrm{ref}}) + \alpha_k\pi$. From (10), we have $\widehat{\mathbf{s}}_{\mathrm{avg}} = \widehat{\mathbf{s}}^{\mathrm{ref}}$. Finally, $\widehat{\phi}_{\mathrm{s}}^{\mathrm{ref}}$, $\widehat{\mathbf{i}}^{\mathrm{ref}}_{\mathrm{lDQ}}$, $\widehat{\gamma}^{\mathrm{ref}}_{\mathrm{DQ}}$, and $\widehat{\xi}^{\mathrm{ref}}_{\mathrm{DQ}}$ can be found by solving the remaining equations in (10). □

Remark 3. *The power-flow equations (12) (13) have been studied extensively and many sufficient conditions for existence and uniqueness of solutions have been developed; e.g., see [4], [30]. Lemma 16 in Appendix restates a useful uniqueness result from [30].*

IV. Stability Analysis of the Dimensionless Grid-tied Inverter-network Dynamics

In bulk power-systems dynamics literature, it is commonplace to assume that the dynamics of the grid-following inverters are much faster than the dynamics of grid-forming inverters and synchronous machines [25]. This assumption justifies the use of a static model for grid-following inverters such that the inverter nodes are considered to be sources of constant (active and reactive) power. Subsequently, the network operation is described by the following power-flow equations:

$$\mathbb{0}_2 = \widehat{s}^{\mathrm{ref}} - \tfrac{3}{2}\mathcal{D}(\widehat{v}_{\mathrm{oDQ}})\widehat{i}_{\mathrm{oDQ}}. \tag{14}$$

Quite obviously, the static representation (14) does not capture stability. The following example shows that the internal dynamics of the inverters can induce instabilities, even if the power-flow equations in (14) admit a high-voltage solution.

Example 4. (**Instabilities Induced by Inverter Dynamics**) *Consider a radial grid-connected network consisting of 25 identical inverters (see Fig. 2 for a sketch). Suppose the inverters have uniform reference power injections $\mathbf{p}^{\mathrm{ref}} = p\mathbb{1}_{25}$, each line has resistance $R = 10^{-2}\ \Omega$ and inductance $L = 10^{-5}$ H, and the grid voltage is $v_{\mathrm{gDQ}} = [0, 120\sqrt{2}]^{\top}$ V(peak) with constant frequency $\omega_{\mathrm{nom}} = 120\pi$ rad/s.*

(i) ***Static model:*** *If inverter power injections satisfy*

$$\widehat{p}\left\|\widehat{Y}_{\mathrm{red}}^{-1}\right\|_{\mathbb{C},\infty} \le \tfrac{3}{8}, \tag{15}$$

then, there exists a unique high-voltage, low-current solution for the power-flow equations (14) (see Lemma 16 in the Appendix).

(ii) ***Dynamic model:*** *We use the dynamic model (5) for the inverters (parameters are given in the fourth column of Table III in Appendix). The governing equations for the network are in (10), and condition (15) via Lemma 2 guarantees the existence of a family of equilibrium points $\widehat{\mathbf{x}}^{\mathrm{ref}}_{\alpha}$, $\alpha \in \mathbb{Z}_2^n$ for the system (10). Linearizing the system (10), we study local stability of $\widehat{\mathbf{x}}^{\mathrm{ref}}_0$.*

Figure 3 plots the maximum real part of the eigenvalues of the linearized system (10) around the equilibrium point $\widehat{\mathbf{x}}^{\mathrm{ref}}_0$ as a function of active-power injection. The red vertical line is the threshold of the power injection for which the power-flow equations admit a unique solution (obtained from (15)). Notice that there are power injections for which a high-voltage solution of the power-flow equations exists, however, the corresponding equilibrium point $\widehat{\mathbf{x}}^{\mathrm{ref}}_0$ is not stable.

A. Small-signal Stability via Time-scale Separation

We now focus on the small-signal stability of the dimensionless grid-tied inverter-network dynamics (10). Due to high dimensionality and nonlinearity of the dynamic model, studying small-signal stability is not analytically tractable. Therefore, it is a reasonable goal to reduce the model order. To that end, we identify a physically meaningful parametrization of the inverters, and we show that under suitable assumptions, this parametrization leads to a time-scale decomposition of the system (10) which simplifies analysis. We begin by uncovering time constants of different sub-systems.

Definition 5 (Singular perturbation parameter)**.** *For dynamics (10), we define:*

$$\epsilon_{\mathrm{I}} = \max\{\|\boldsymbol{\tau}_{\mathrm{PLL}}\|_{\infty}, \|\boldsymbol{\tau}'_{\mathrm{PLL}}\|_{\infty}, \|\boldsymbol{\tau}_{\mathrm{s}}\|_{\infty}, \|\mathbf{T}_{\mathrm{s}}\|_{\infty}, \|\mathbf{T}_{\mathrm{PLL}}\|_{\infty},$$
$$\|\boldsymbol{\tau}_{\mathrm{c}}\|_{\infty}^{\frac{1}{2}}, \|\mathbf{T}_{\mathrm{c}}\|_{\infty}^{\frac{1}{2}}\},$$
$$\epsilon_{\mathcal{E}} = \max\left\{\|\boldsymbol{\tau}_{\mathrm{LC}}\|_{\infty}^{\frac{1}{2}}, \|\boldsymbol{\tau}'_{\mathrm{LC}}\|_{\infty}^{\frac{1}{2}}, \|\boldsymbol{\tau}_{\mathcal{E}}\|_{\infty}^{\frac{1}{2}}\right\}.$$

Using these, we define the singular perturbation parameter*:*

$$\epsilon := \max\{\epsilon_{\mathrm{I}}, \epsilon_{\mathcal{E}}\}. \tag{16}$$

Remark 6. *(i) Definition 5 establishes a physically meaningful time-scale separation of the components of the inverter network when $\epsilon \ll 1$. In this case, $\|\boldsymbol{\tau}'_{\mathrm{LC}}\|_{\infty}, \|\boldsymbol{\tau}_{\mathrm{LC}}\|_{\infty}, \|\boldsymbol{\tau}_{\mathcal{E}}\|_{\infty}, \|\boldsymbol{\tau}_{\mathrm{c}}\|_{\infty}, \|\mathbf{T}_{\mathrm{c}}\|_{\infty} \le \epsilon^2$ which implies that the line dynamics, the LC filter, and the current controller are the fastest components. Moreover, $\|\boldsymbol{\tau}_{\mathrm{PLL}}\|_{\infty}, \|\boldsymbol{\tau}'_{\mathrm{PLL}}\|_{\infty}, \|\boldsymbol{\tau}_{\mathrm{s}}\|_{\infty} \le \epsilon$ which implies that the PLL, and averaging-part of the power controller (i.e., $\widehat{\mathbf{s}}_{\mathrm{avg}}$) are slower than the current controller, the line dynamics, and the LC filter but they are faster than the power-tracking controller (i.e., $\widehat{\phi}_{\mathrm{s}}$) dynamics.*

(ii) The assumption $\epsilon \ll 1$ is equivalent to $\epsilon_{\mathrm{I}}, \epsilon_{\mathcal{E}} \ll 1$, which is realistic in practice. For instance, in the inverter models with the parameters in Table III in Appendix and those used in [17], [22], [23], it holds that $\epsilon_{\mathrm{I}}, \epsilon_{\mathcal{E}} \le 0.1$.

(iii) $\tau_e = \frac{L_{\mathrm{e}}}{\sqrt{R_{\mathrm{e}}^2 + \omega_{\mathrm{nom}}^2 L_{\mathrm{e}}^2}} \le \omega_{\mathrm{nom}}^{-1}$, for every $e \in \mathcal{E}$. Similarly, one can show that $\|\boldsymbol{\tau}'_{\mathrm{LC}}\|_{\infty}, \|\boldsymbol{\tau}_{\mathrm{LC}}\|_{\infty} \le \omega_{\mathrm{nom}}^{-\frac{1}{2}}$ and this gives an upper bound for the LC and line parameter $\epsilon_{\mathcal{E}} \le \omega_{\mathrm{nom}}^{-\frac{1}{2}}$.

(iv) For different parameters and control architectures, one can conceivably identify a different singular perturbation parameter and time-scale decomposition. However, we expect the corresponding stability result to be similar.

2325-5870 (c) 2021 IEEE. Personal use is permitted, but republication/redistribution requires IEEE permission. See http://www.ieee.org/publications_standards/publications/rights/index.html for more information.
Authorized licensed use limited to: University of Washington Libraries. Downloaded on April 19,2022 at 20:42:08 UTC from IEEE Xplore. Restrictions apply.

This article has been accepted for publication in a future issue of this journal, but has not been fully edited. Content may change prior to final publication. Citation information: DOI 10.1109/TCNS.2021.3084444, IEEE Transactions on Control of Network Systems

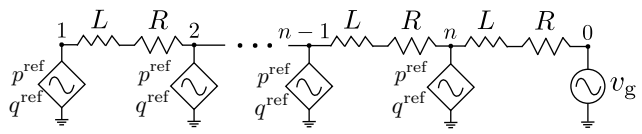

Fig. 2: A radial network with n inverters connected to the grid bus.

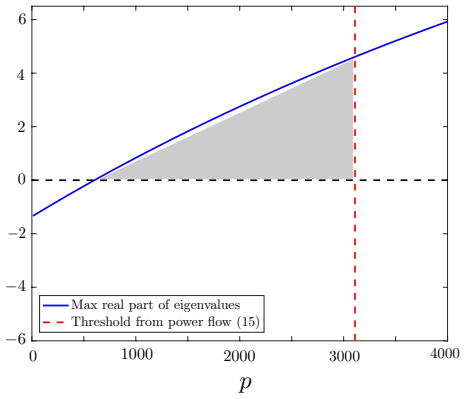

Fig. 3: Shaded region shows power injections that admit a unique power flow solution that is, however, not small-signal stable.

Theorem 7 (Small-signal Stability)**.** *Consider the dimensionless grid-tied inverter-network dynamics* (10) *with states in* $\mathbb{R}^{13n+2m}$ *and references* $\widehat{\mathbf{s}}^{\mathrm{ref}} \in \mathbb{R}^{2n}$*. The following hold:*

(i) if

$$\left\| \mathcal{D}'(\widehat{\mathbf{w}}) \widehat{Y}_{\mathrm{red}}^{-1} (\mathcal{D}'(\widehat{\mathbf{w}}))^{-1} \mathcal{D}'(\widehat{\mathbf{s}}^{\mathrm{ref}}) \right\|_{\mathbb{C},\infty} \leq \tfrac{3}{8}, \tag{17}$$

then there is a unique solution $((\widehat{\mathbf{v}}_{\mathrm{oDQ}}^{\mathrm{ref}})^\top, (\widehat{\mathbf{i}}_{\mathrm{oDQ}}^{\mathrm{ref}})^\top)^\top$ *for the power-flow equations* (12) *and* (13) *and a family of equilibrium points* $\widehat{\mathbf{x}}_\alpha^{\mathrm{ref}}$*,* $\alpha \in \mathbb{Z}_2^n$*, for the grid-tied inverter network dynamics* (10) *satisfying:*

$$\left\| \widehat{\mathbf{v}}_{\mathrm{oDQ}}^{\mathrm{ref}} - \widehat{\mathbf{w}} \right\|_{\mathbb{C},\infty} \leq \tfrac{1}{2} \|\widehat{\mathbf{w}}\|_{\mathbb{C},\infty};$$

(ii) if the equilibrium point $\widehat{\mathbf{x}}_0^{\mathrm{ref}}$ *for the inverter network* (10) *exists,* $[\mathbf{T}_{\mathrm{PLL}}] \succ [\boldsymbol{\tau}_{\mathrm{PLL}}]$*, and the* $2n \times 2n$ *matrix*

$$M := -\Big(\mathcal{D}(\widehat{\mathbf{v}}_{\mathrm{oDQ}}^{\mathrm{ref}}) \widehat{Y}_{\mathrm{red}} + \mathcal{D}'(\widehat{\mathbf{i}}_{\mathrm{oDQ}}^{\mathrm{ref}}) \Big) \times \widehat{Y}_{\mathrm{C,red}}^{-1} \mathbf{R}(-\boldsymbol{\delta}^{\mathrm{ref}}) \mathcal{H} [\boldsymbol{\tau}'_{\mathrm{s}} \otimes I_2]^{-1} \tag{18}$$

is Hurwitz. Then, there exists an $\epsilon^* > 0$ *such that, for every* $\epsilon \leq \epsilon^*$*, the equilibrium point* $\widehat{\mathbf{x}}_0^{\mathrm{ref}}$ *is locally exponentially stable.*

Proof. Regarding part (i), the proof follows from combining Lemma 16 in Appendix and Lemma 2. Regarding part (ii), consider the dimensionless grid-tied inverter network dynamics (10). In order to perform the three time-scale singular perturbation, we introduce the small variable $\sigma = \epsilon^2$. Then it is clear that $\sigma \ll \epsilon \ll 1$ and they induce a three-time-scale separation for the dynamical system (10). Using (16) and defining the variable $\Delta\mathbf{x} \in \mathbb{R}^{13n+2m}$ by $\Delta\mathbf{x} = \mathbf{x} - \mathbf{x}_0^{\mathrm{ref}}$, we get a three-time-scale decomposition of the system. We define the states $\mathbf{z}_1 \in \mathbb{R}^{6n+2m}$, $\mathbf{z}_2 \in \mathbb{R}^{5n}$, and $\mathbf{z}_3 \in \mathbb{R}^{2n}$ as follows:

$$\mathbf{z}_1 = \begin{pmatrix} \Delta\widehat{\boldsymbol{\gamma}}_{\mathrm{DQ}} & \Delta\widehat{\mathbf{i}}_{\mathrm{lDQ}} & \Delta\widehat{\mathbf{v}}_{\mathrm{oDQ}} & \Delta\xi_{\mathrm{DQ}} \end{pmatrix}^\top,$$

$$\mathbf{z}_2 = \begin{pmatrix} \Delta\widehat{\mathbf{v}}_{\mathrm{PLL}} & \Delta\widehat{\boldsymbol{\phi}}_{\mathrm{PLL}} & \Delta\boldsymbol{\delta} & \Delta\widehat{\mathbf{s}}_{\mathrm{avg}} \end{pmatrix}^\top,$$

$$\mathbf{z}_3 = \mathcal{R}(-\boldsymbol{\delta}) \mathcal{H} \widehat{\boldsymbol{\phi}}_{\mathrm{s}} - \mathcal{R}(-\boldsymbol{\delta}^{\mathrm{ref}}) \mathcal{H} \widehat{\boldsymbol{\phi}}_{\mathrm{s}}^{\mathrm{ref}},$$

where $\mathbf{z}_1$ is *faster* than $\mathbf{z}_2$ and $\mathbf{z}_2$ are *faster* than $\mathbf{z}_3$. Note that the variable $\mathbf{z}_1$ includes the states of the current controller and the inductor currents and the capacitor voltages in the filters and the current flows in the lines, the variable $\mathbf{z}_2$ includes the output phase angle and the states of low-pass filter and PI controller in the PLL and the state of low-pass filter in the power control loop, and the variable $\mathbf{z}_3$ includes the state of PI controller in the power control loop. The corresponding time-scales are given by $\tau = t/\sigma$ and $\tau' = t/\epsilon$. Using these time scales, the dimensionless grid-tied inverter network dynamics (10) can be written as follows:

$$\begin{aligned} \dot{\mathbf{z}}_3 &= g_3(\mathbf{z}_1, \mathbf{z}_2, \mathbf{z}_3, \epsilon), \\ \epsilon \dot{\mathbf{z}}_2 &= g_2(\mathbf{z}_1, \mathbf{z}_2, \mathbf{z}_3), \\ \sigma \dot{\mathbf{z}}_1 &= g_1(\mathbf{z}_1, \mathbf{z}_2, \mathbf{z}_3, \sigma), \end{aligned} \tag{19}$$

where g_1, g_2, g_3 are suitably defined functions. Note that, by Lemma 2, the equilibrium point $\mathbf{x}_0^{\mathrm{ref}}$ of the dimensionless grid-tied inverter network (10) is independent of both σ and ϵ. As a result, $(\mathbf{z}_1^\top, \mathbf{z}_2^\top, \mathbf{z}_3^\top)^\top = \mathbb{0}_{13n+2m}$ is an equilibrium point for (19) for every $\sigma, \epsilon > 0$. Our proof strategy is based on successive use of singular perturbation with respect to the time-scales τ and τ'. The quasi-steady-state manifold for the time-scale τ is the manifold $\mathbf{z}_1 = h_1(\mathbf{z}_2, \mathbf{z}_3)$ obtained by solving the algebraic equations $g_1(\mathbf{z}_1, \mathbf{z}_2, \mathbf{z}_3, 0) = \mathbb{0}_{(6n+2m)}$ [11, §11.2]. After some algebraic computations, the quasi-steady-state manifold for the time-scale τ is given by:

$$\begin{aligned} \Delta\widehat{\boldsymbol{\gamma}}_{\mathrm{DQ}} &= \widehat{Y}_{\mathrm{C,red}}^{-1} \Big(\mathcal{R}(-\boldsymbol{\delta}) \mathcal{H} \widehat{\boldsymbol{\phi}}_{\mathrm{s}} - \mathcal{R}(-\boldsymbol{\delta}^{\mathrm{ref}}) \mathcal{H} \widehat{\boldsymbol{\phi}}_{\mathrm{s}}^{\mathrm{ref}} \Big) = \widehat{Y}_{\mathrm{C,red}}^{-1} \mathbf{z}_3, \\ \Delta\widehat{\mathbf{i}}_{\mathrm{lDQ}} &= \mathcal{R}(-\boldsymbol{\delta}) \mathcal{H} \widehat{\boldsymbol{\phi}}_{\mathrm{s}} - \mathcal{R}(-\boldsymbol{\delta}^{\mathrm{ref}}) \mathcal{H} \widehat{\boldsymbol{\phi}}_{\mathrm{s}}^{\mathrm{ref}} = \mathbf{z}_3, \\ \Delta\widehat{\mathbf{v}}_{\mathrm{oDQ}} &= \widehat{Y}_{\mathrm{C,red}}^{-1} \Big(\mathcal{R}(-\boldsymbol{\delta}) \mathcal{H} \widehat{\boldsymbol{\phi}}_{\mathrm{s}} - \mathcal{R}(-\boldsymbol{\delta}^{\mathrm{ref}}) \mathcal{H} \widehat{\boldsymbol{\phi}}_{\mathrm{s}}^{\mathrm{ref}} \Big) = \widehat{Y}_{\mathrm{C,red}}^{-1} \mathbf{z}_3, \\ \Delta\widehat{\xi}_{\mathrm{DQ}} &= \mathcal{Z}_{\mathrm{L}}^{-1} (B_{\mathrm{I}}^\top \otimes I_2) \widehat{Y}_{\mathrm{C,red}}^{-1} \mathbf{z}_3. \end{aligned}$$

Since the quasi-steady-state manifold for the time-scale τ is an isolated manifold, the singular perturbation problem is in the standard form. Now, we introduce the error variables $\mathbf{e}_1, \mathbf{e}_2, \mathbf{e}_3 \in \mathbb{R}^{2n}$ and $\mathbf{e}_4 \in \mathbb{R}^{2m}$ as follows:

$$\mathbf{e}_1 = \Delta\widehat{\boldsymbol{\gamma}}_{\mathrm{DQ}} - \widehat{Y}_{\mathrm{C,red}}^{-1} \mathbf{z}_3, \tag{20}$$

$$\mathbf{e}_2 = \Delta\widehat{\mathbf{i}}_{\mathrm{lDQ}} - \mathbf{z}_3, \tag{21}$$

$$\mathbf{e}_3 = \Delta\widehat{\mathbf{v}}_{\mathrm{oDQ}} - \widehat{Y}_{\mathrm{C,red}}^{-1} \mathbf{z}_3, \tag{22}$$

$$\mathbf{e}_4 = \Delta\widehat{\xi}_{\mathrm{DQ}} - \mathcal{Z}_{\mathrm{L}}^{-1} (B_{\mathrm{I}}^\top \otimes I_2) \widehat{Y}_{\mathrm{C,red}}^{-1} \mathbf{z}_3. \tag{23}$$

Using these error variables, the boundary-layer dynamics associated to the time-scale τ are:

$$\frac{d\mathbf{e}_1}{d\tau} = -\sigma [\boldsymbol{\tau}_{\mathrm{c}} \otimes I_2]^{-1} \mathbf{e}_2 \tag{24a}$$

$$\frac{d\mathbf{e}_2}{d\tau} = \sigma ([\boldsymbol{\tau}_{\mathrm{LC}}]^{-1} [\mathcal{X}] \otimes I_2)(\mathbf{e}_1 - \mathbf{e}_3 - ([\boldsymbol{\tau}_{\mathrm{c}}]^{-1} [\mathbf{T}_{\mathrm{c}}] \otimes I_2) \mathbf{e}_2), \tag{24b}$$

$$\frac{d\mathbf{e}_3}{d\tau} = \sigma ([\boldsymbol{\tau}'_{\mathrm{LC}}][\mathcal{X}] \otimes I_2)^{-1} \Big(\mathbf{e}_2 - (B_{\mathrm{I}} \otimes I_2) \mathbf{e}_4 - [\boldsymbol{\tau}''_{\mathrm{LC}} \otimes I_2] \mathbf{e}_3 \Big), \tag{24c}$$

$$\frac{d\mathbf{e}_4}{d\tau} = \sigma ([\boldsymbol{\tau}_{\mathcal{E}}][\boldsymbol{\tau}'_{\mathcal{E}}] \otimes I_2)^{-1} ((B_{\mathrm{I}}^\top \otimes I_2) \mathbf{e}_3 - \mathcal{Z}_{\mathrm{L}} \mathbf{e}_4). \tag{24d}$$

2325-5870 (c) 2021 IEEE. Personal use is permitted, but republication/redistribution requires IEEE permission. See http://www.ieee.org/publications_standards/publications/rights/index.html for more information.
Authorized licensed use limited to: University of Washington Libraries. Downloaded on April 19,2022 at 20:42:08 UTC from IEEE Xplore. Restrictions apply.

This article has been accepted for publication in a future issue of this journal, but has not been fully edited. Content may change prior to final publication. Citation information: DOI 10.1109/TCNS.2021.3084444, IEEE Transactions on Control of Network Systems

We first show that for the boundary-layer dynamics (24), the origin is the exponentially stable equilibrium point. It is easy to see that since the graph is connected, we have $\mathrm{Ker}(B_{\mathrm{I}}^{\top}) = \{\mathbb{0}_n\}$, the matrix $([\boldsymbol{\tau}''_{\mathrm{LC}} \otimes I_2])\mathcal{J}$ is skew-symmetric and the matrix $-(\mathcal{Z}_{\mathrm{L}} + \mathcal{Z}_{\mathrm{L}}^{\top})$ is negative definite. Hence, using Lemma 15 in Appendix, the origin is the locally exponentially stable point of the boundary-layer dynamics (24). Using [11, Theorem 11.4], the dynamical system (19) is locally exponentially stable around the origin, if the reduced-order system:

$$\begin{aligned} \dot{\mathbf{z}}_3 &= g_3(h_1(\mathbf{z}_2, \mathbf{z}_3), \mathbf{z}_2, \mathbf{z}_3, \epsilon), \\ \epsilon \dot{\mathbf{z}}_2 &= g_2(h_1(\mathbf{z}_2, \mathbf{z}_3), \mathbf{z}_2, \mathbf{z}_3), \end{aligned} \tag{25}$$

is locally exponentially stable around the origin. Now, we use singular perturbation analysis with respect to the time-scale τ' to show that the dynamical system (25) is locally exponentially stable around the origin. Note that, the quasi-steady-state manifold for time-scale τ' is $\mathbf{z}_2 = h_2(\mathbf{z}_3)$ obtained by solving the algebraic equations $g_2(h_1(\mathbf{z}_2, \mathbf{z}_3), \mathbf{z}_2, \mathbf{z}_3) = \mathbb{0}_{5n}$. Thus, the quasi-steady-state manifold for time-scale τ' is given by:

$$\begin{aligned} &\Delta\widehat{\mathbf{v}}_{\mathrm{PLL}} = \mathbb{0}_n,\ \Delta\widehat{\boldsymbol{\phi}}_{\mathrm{PLL}} = \mathbb{0}_n,\ \Delta\boldsymbol{\delta} = \boldsymbol{\delta}^{BL}(\mathbf{z}_3) - \arg(\widehat{\mathbf{v}}^{\mathrm{ref}}_{\mathrm{oDQ}}), \\ &\Delta\widehat{\mathbf{s}}_{\mathrm{avg}} = \tfrac{3}{2}\mathcal{D}\big(\widehat{Y}^{-1}_{\mathrm{C,red}}\mathbf{z}_3 + \widehat{\mathbf{v}}^{\mathrm{ref}}_{\mathrm{oDQ}}\big)\left(\widehat{Y}_{\mathrm{red}}\widehat{Y}^{-1}_{\mathrm{C,red}}\mathbf{z}_3 + \widehat{\mathbf{i}}^{\mathrm{ref}}_{\mathrm{oDQ}}\right) - \mathbf{s}^{\mathrm{ref}}. \end{aligned}$$

where $\boldsymbol{\delta}^{BL} : \mathbb{R}^{2n} \to \mathbb{R}^n$ is defined by $\boldsymbol{\delta}^{BL}(\mathbf{z}_3) = \arg\left(\widehat{Y}^{-1}_{\mathrm{C,red}}\left(\mathbf{z}_3 + \mathcal{R}(-\boldsymbol{\delta}^{\mathrm{ref}})\mathcal{H}\widehat{\boldsymbol{\phi}}^{\mathrm{ref}}_{\mathrm{s}}\right)\right)$. Since the quasi-steady state manifold for the time-scale τ' is an isolated manifold, the singular perturbation problem is in the standard form. We introduce the error variables $\mathbf{e}_5, \mathbf{e}_6, \mathbf{e}_7 \in \mathbb{R}^n$ and $\mathbf{e}_8 \in \mathbb{R}^{2n}$:

$$\begin{aligned} \mathbf{e}_5 &= \Delta\widehat{\mathbf{v}}_{\mathrm{PLL}}, \mathbf{e}_6 = \Delta\widehat{\boldsymbol{\phi}}_{\mathrm{PLL}} \\ \mathbf{e}_7 &= \Delta\boldsymbol{\delta} - \boldsymbol{\delta}^{BL}(\mathbf{z}_3) + \arg(\widehat{\mathbf{v}}^{\mathrm{ref}}_{\mathrm{oDQ}}) \\ \mathbf{e}_8 &= \Delta\widehat{\mathbf{s}}_{\mathrm{avg}} - \tfrac{3}{2}\mathcal{D}\big(\widehat{Y}^{-1}_{\mathrm{C,red}}\mathbf{z}_3 + \widehat{\mathbf{v}}^{\mathrm{ref}}_{\mathrm{oDQ}}\big) \\ &\quad \left(\widehat{Y}_{\mathrm{red}}\widehat{Y}^{-1}_{\mathrm{C,red}}\mathbf{z}_3 + \widehat{\mathbf{i}}^{\mathrm{ref}}_{\mathrm{oDQ}}\right) + \mathbf{s}^{\mathrm{ref}}. \end{aligned}$$

Thus, the boundary-layer dynamics associated to the time-scale τ' is given by:

$$\frac{d\mathbf{e}_5}{d\tau'} = \epsilon[\boldsymbol{\tau}_{\mathrm{PLL}}]^{-1}(\Delta\widehat{\mathbf{v}}_{\mathrm{od}} - \mathbf{e}_5), \frac{d\mathbf{e}_6}{d\tau'} = -\epsilon[\mathbf{T}_{\mathrm{PLL}}]^{-1}\mathbf{e}_5, \tag{26a}$$

$$\frac{d\mathbf{e}_7}{d\tau'} = \epsilon[\boldsymbol{\tau}'_{\mathrm{PLL}}]^{-1}(\mathbf{e}_6 - \mathbf{e}_5), \tag{26b}$$

$$\frac{d\mathbf{e}_8}{d\tau'} = -\epsilon[\boldsymbol{\tau}_{\mathrm{s}} \otimes I_2]^{-1}\mathbf{e}_8, \tag{26c}$$

where $\Delta\widehat{\mathbf{v}}_{\mathrm{od}}$ is the d-component of $\mathcal{R}(\boldsymbol{\delta})\left(\widehat{Y}^{-1}_{\mathrm{C,red}}\mathbf{z}_3 + \widehat{\mathbf{v}}^{\mathrm{ref}}_{\mathrm{oDQ}}\right) - \widehat{\mathbf{v}}^{\mathrm{ref}}_{\mathrm{odq}}$. We show that the boundary-layer dynamics (26) are stable around the origin. Let $\mathbf{e} = (\mathbf{e}_5^{\top}, \mathbf{e}_6^{\top}, \mathbf{e}_7^{\top}, \mathbf{e}_8^{\top})^{\top} \in \mathbb{R}^{5n}$. Note that the linearized boundary-layer equation dynamics around the origin have the form $\Delta\dot{\mathbf{e}} = S\Delta\mathbf{e}$, where $S \in \mathbb{R}^{5n\times 5n}$ has the upper block triangular form $S = \begin{pmatrix} S_{11} & S_{12} \\ \mathbb{0}_{2n\times 3n} & S_{22} \end{pmatrix}$ with:

$$S_{11} = \begin{pmatrix} -\epsilon[\boldsymbol{\tau}_{\mathrm{PLL}}]^{-1} & \mathbb{0}_{n\times n} & \epsilon[\boldsymbol{\tau}_{\mathrm{PLL}}]^{-1}[\widehat{\mathbf{v}}_{\mathrm{oq}}] \\ -\epsilon[\mathbf{T}_{\mathrm{PLL}}]^{-1} & \mathbb{0}_{n\times n} & \mathbb{0}_{n\times n} \\ -\epsilon[\boldsymbol{\tau}'_{\mathrm{PLL}}]^{-1} & \epsilon[\boldsymbol{\tau}'_{\mathrm{PLL}}]^{-1} & \mathbb{0}_{n\times n} \end{pmatrix},$$

$$S_{22} = -\epsilon[\boldsymbol{\tau}_{\mathrm{s}} \otimes I_2]^{-1}.$$

Note that $\widehat{\mathbf{v}}_{\mathrm{odq}} = \mathcal{R}(\boldsymbol{\delta})\widehat{Y}^{-1}_{\mathrm{C,red}}\mathbf{z}_3 + \widehat{\mathbf{v}}^{\mathrm{ref}}_{\mathrm{odq}}$. By Lemma 2, we know that $\widehat{\mathbf{v}}^{\mathrm{ref}}_{\mathrm{oq}} > \mathbb{0}_n$. This implies that, for $\mathbf{z_3}$ close enough to the origin, we get $\widehat{\mathbf{v}}_{\mathrm{oq}} > \mathbb{0}_n$. Moreover, we have $[\mathbf{T}_{\mathrm{PLL}}] \succ [\boldsymbol{\tau}_{\mathrm{PLL}}]$. Using Lemma 15 in Appendix, the matrix S is Hurwitz. Therefore, the origin is the locally exponentially stable point of the boundary-layer equations (26). Now, we consider the reduced-order dynamics. The reduced-order model for the multi-time-scale analysis is given by:

$$\dot{\mathbf{z}}_3 = g_3(h_1(h_2(\mathbf{z}_3), \mathbf{z}_3), h_2(\mathbf{z}_3), \mathbf{z}_3, 0). \tag{27}$$

In order to study the stability of the reduced-order model (27), note that $\mathbf{z}_3 = \mathcal{R}(-\boldsymbol{\delta})\mathcal{H}\widehat{\boldsymbol{\phi}}_{\mathrm{s}} - \mathcal{R}(-\boldsymbol{\delta}^{\mathrm{ref}})\mathcal{H}\widehat{\boldsymbol{\phi}}^{\mathrm{ref}}_{\mathrm{s}}$. This implies that the reduced order model (27) is given by:

$$\begin{aligned} \dot{\mathbf{z}}_3 = -\tfrac{3}{2}\mathcal{R}(-\boldsymbol{\delta}^{\mathrm{ref}})\mathcal{H}[\boldsymbol{\tau}'_{\mathrm{s}} \otimes I_2]^{-1}\mathcal{D}\big(\widehat{Y}^{-1}_{\mathrm{C,red}}\mathbf{z}_3 + \widehat{\mathbf{v}}^{\mathrm{ref}}_{\mathrm{oDQ}}\big)\times \\ \left(\widehat{Y}_{\mathrm{red}}\widehat{Y}^{-1}_{\mathrm{C,red}}\mathbf{z}_3 + \widehat{\mathbf{i}}^{\mathrm{ref}}_{\mathrm{oDQ}}\right). \end{aligned}$$

Linearizing the above equation, we get $\Delta\dot{\mathbf{z}}_3 = M'\Delta\mathbf{z}_3$, where

$$\begin{aligned} M' := -\tfrac{3}{2}\mathcal{R}(-\boldsymbol{\delta}^{\mathrm{ref}})\mathcal{H}[\boldsymbol{\tau}'_{\mathrm{s}} \otimes I_2]^{-1}\times \\ \left(\mathcal{D}(\widehat{\mathbf{v}}^{\mathrm{ref}}_{\mathrm{oDQ}})\widehat{Y}_{\mathrm{red}} + \mathcal{D}'(\widehat{\mathbf{i}}^{\mathrm{ref}}_{\mathrm{oDQ}})\right)\widehat{Y}^{-1}_{\mathrm{C,red}}. \end{aligned}$$

Note that, for any scalar $c \in \mathbb{R}_{>0}$ and any matrix $A \in \mathbb{R}^{2n\times 2n}$, the matrix A is Hurwitz if and only if the matrix cA is Hurwitz. Moreover, by [10, Theorem 1.3.22], Hurwitzness of the matrix M' is equivalent to the Hurwitzness of matrix M defined in (18). This means that M' is Hurwitz and the origin is a locally exponentially stable equilibrium point of the reduced-order model (27) associated to the time-scale τ'. Note that the boundary-layer dynamics associated with the time-scale τ' are given by (26) and are shown to be locally exponentially stable around the origin. Thus, using [11, Theorem 11.4], there exists $\widehat{\epsilon} > 0$ such that, for every $\epsilon \leq \widehat{\epsilon}$, the reduced-order dynamics (25) associated to the time-scale τ are locally exponentially stable around the origin. Note that the boundary-layer dynamics associated to the time-scale τ are given by (24) and shown to be locally exponentially stable around the origin. Therefore, using [11, Theorem 11.4] for the time-scale τ, there exists $\widehat{\sigma} > 0$ such that, for every $\sigma \leq \widehat{\sigma}$ and $\epsilon \leq \widehat{\epsilon}$, the dynamical system (19) is locally exponentially stable around the origin. By defining $\epsilon^* = \min\{\sqrt{\widehat{\sigma}}, \widehat{\epsilon}\}$, the stability of the equilibrium point of the dimensionless network dynamics follows from condition *(ii)* for every $\epsilon \leq \epsilon^*$. □

Remark 8. *(1) The largest value of ϵ^* for which Theorem 7(ii) holds is hard to compute. A standard lower bound on ϵ^* can be obtained via [12, Lemma 2.2].*

(2) In [17], small-signal stability of inverter networks has been studied using eigenvalue analysis for the full-order systems. For large-scale networks, eigenvalue analysis of the grid-tied inverter network dynamics (10) is computationally complicated and, in general, it requires linearizing the system (10) and checking stability of a $(13n + 2m)$-dimensional matrix. Theorem 7(ii) uses a time-scale analysis to eliminate the line dynamics, the dynamics of the current controller, PLL, and LC filter from small-signal stability analysis. The sufficient condition in Theorem 7(ii) significantly reduces computational complexity by reducing the problem to checking that a $2n$-dimensional matrix is Hurwitz;

2325-5870 (c) 2021 IEEE. Personal use is permitted, but republication/redistribution requires IEEE permission. See http://www.ieee.org/publications_standards/publications/rights/index.html for more information.
Authorized licensed use limited to: University of Washington Libraries. Downloaded on April 19,2022 at 20:42:08 UTC from IEEE Xplore. Restrictions apply.

This article has been accepted for publication in a future issue of this journal, but has not been fully edited. Content may change prior to final publication. Citation information: DOI 10.1109/TCNS.2021.3084444, IEEE Transactions on Control of Network Systems

(3) By part (i), there exists a family of equilibrium point $\widehat{\mathbf{x}}^{\mathrm{ref}}_{\alpha}$ for the grid-tied inverter network dynamics (10). However, in part (ii), we focus on the equilibrium point $\widehat{\mathbf{x}}^{\mathrm{ref}}_{0}$. The reason is that this trajectory is locally exponentially stable when there is no power injection for the inverters;

(4) Theorem 7(ii) brings out the role of network topology, the power injections/demands, and inverter parameters in small-signal stability of inverter networks. For the matrix M, the term $\widehat{Y}_{\mathrm{red}}$ reveals the role of network topology. The terms $\widehat{\mathbf{i}}^{\mathrm{ref}}_{\mathrm{oDQ}}$, $\widehat{\mathbf{v}}^{\mathrm{ref}}_{\mathrm{oDQ}}$, and δ^{ref} (obtained by solving the power-flow equations (12)–(13)) reveal the role of network topology and power injections/demands. Finally, $\boldsymbol{\tau}'_{\mathrm{s}}$ reveals the role of inverters' internal dynamics.

B. Corollaries

Corollary 9 (Single inverter connected to the grid)**.** *Consider a single inverter with the reference power injection $s^{\mathrm{ref}} = (p^{\mathrm{ref}}, q^{\mathrm{ref}})^{\top}$ connected to the grid with voltage $v_{\mathrm{gDQ}} = \left(\begin{smallmatrix} 0 \\ V_{\mathrm{g}} \end{smallmatrix}\right)$ through a line with resistance R and inductance L. If*

$$\|s^{\mathrm{ref}}\|_2 \leq \tfrac{3}{8}\frac{V_{\mathrm{g}}^2}{\sqrt{R^2+\omega_{\mathrm{nom}}^2 L^2}}, \tag{28}$$

(i) there exist two equilibrium points $\widehat{\mathrm{x}}^{\mathrm{ref}}_0$ and $\widehat{\mathrm{x}}^{\mathrm{ref}}_1$ satisfying

$$\|\widehat{v}^{\mathrm{ref}}_{\mathrm{oDQ}} - \left(\begin{smallmatrix} 0 \\ 1 \end{smallmatrix}\right)\|_{\mathbb{C},\infty} \leq \tfrac{1}{2};$$

(ii) if we have $\mathrm{T}_{\mathrm{PLL}} > \tau_{\mathrm{PLL}}$, then there exists a $\epsilon^* > 0$ such that, for every $\epsilon \leq \epsilon^*$, $\widehat{\mathrm{x}}^{\mathrm{ref}}_0$ is locally exponentially stable.

Proof. Regarding part (i), we define the dimensionless resistance $\widehat{R} = V_{\mathrm{g}}^{-2} s_{\mathrm{nom}} R$ and dimensionless inductance $\widehat{L} = V_{\mathrm{g}}^{-2} s_{\mathrm{nom}} L$. Therefore, we get $\widehat{Y}^{-1}_{\mathrm{red}} = \begin{pmatrix} \widehat{R} & -\omega_{\mathrm{nom}}\widehat{L} \\ \omega_{\mathrm{nom}}\widehat{L} & \widehat{R} \end{pmatrix}$. Then, (28) is equivalent to (17) and the result follows from Theorem 7(i). Regarding part (ii), note that we have $\widehat{\mathrm{v}}^{\mathrm{ref}}_{\mathrm{oDQ}} - (\widehat{R}I_2 + \omega_{\mathrm{nom}}\widehat{L}\mathcal{J})\widehat{\mathrm{i}}^{\mathrm{ref}}_{\mathrm{oDQ}} = \left(\begin{smallmatrix} 0 \\ 1 \end{smallmatrix}\right)$. Then, matrix M in (18) becomes:

$$\begin{aligned} M &= -\Big(\mathcal{D}(\widehat{\mathrm{v}}^{\mathrm{ref}}_{\mathrm{oDQ}}) + \mathcal{D}'(\widehat{\mathrm{i}}^{\mathrm{ref}}_{\mathrm{oDQ}})\widehat{Y}^{-1}_{\mathrm{red}}\Big)\mathcal{HR}(-\delta^{\mathrm{ref}})[\tau'_{\mathrm{s}} \otimes I_2]^{-1} \\ &= -\begin{pmatrix} 2\widehat{R}\widehat{i}^{\mathrm{ref}}_{\mathrm{oD}} & 1+2\widehat{R}\widehat{i}^{\mathrm{ref}}_{\mathrm{oQ}} \\ 1+2\omega_{\mathrm{nom}}\widehat{L}\widehat{i}^{\mathrm{ref}}_{\mathrm{oD}} & 2\omega_{\mathrm{nom}}\widehat{L}\widehat{i}^{\mathrm{ref}}_{\mathrm{oQ}} \end{pmatrix}\mathcal{HR}(-\delta^{\mathrm{ref}})(\tau'_{\mathrm{s}})^{-1}. \end{aligned}$$

Using simple algebraic manipulations, we get $\det(M) = (2\widehat{v}^{\mathrm{ref}}_{\mathrm{oQ}} - 1)(\tau'_{\mathrm{s}})^{-1}$ and $\mathrm{tr}(M) = -2\widehat{v}^{\mathrm{ref}}_{\mathrm{oq}}(\tau'_{\mathrm{s}})^{-1}$. Since $\|\widehat{\mathrm{v}}^{\mathrm{ref}}_{\mathrm{oDQ}} - \left(\begin{smallmatrix} 0 \\ 1 \end{smallmatrix}\right)\|_2 \leq \frac{1}{2}$, we have $2\widehat{v}^{\mathrm{ref}}_{\mathrm{oQ}} \geq 1$. This implies that $\det(M) \geq 0$. Moreover, for the equilibrium points $\widehat{\mathrm{x}}^{\mathrm{ref}}_0$, we have $\widehat{v}^{\mathrm{ref}}_{\mathrm{oq}} > 0$. This implies that $\mathrm{tr}(M) < 0$ and M is Hurwitz. Thus, by Theorem 7(ii), $\widehat{\mathrm{x}}^{\mathrm{ref}}_0$ is locally exponentially stable. □

In the next corollary, we study the special case of resistive networks and provide a computationally efficient numerical method for checking sufficient condition (18).

Corollary 10 (Resistive network of inverters)**.** *Consider the dynamics (10). Suppose the lines are purely resistive and the reference power injections and demands are purely active. The following statements hold:*

(i) if $\Big\|[\widehat{\mathbf{u}}]\widehat{L}^{-1}_{\mathrm{red}}[\widehat{\mathbf{u}}]^{-1}[\widehat{\mathbf{p}}^{\mathrm{ref}}]\Big\|_{\mathbb{C},\infty} \leq \frac{3}{8}$, where $\widehat{\mathbf{u}} = \widehat{L}^{-1}_{\mathrm{red}}\widehat{L}_{0\mathrm{g}}v_{\mathrm{gDQ}}$, then there exists a family of equilibrium points $\widehat{\mathbf{x}}^{\mathrm{ref}}_{\alpha}$ for (10) with the property that

$$\big\|\widehat{\mathbf{v}}^{\mathrm{ref}}_{\mathrm{oDQ}} - \widehat{\mathbf{w}}\big\|_{\mathbb{C},\infty} \leq \tfrac{1}{2}\|\widehat{\mathbf{w}}\|_{\mathbb{C},\infty};$$

(ii) if additionally $[\mathbf{T}_{\mathrm{PLL}}] \succ [\boldsymbol{\tau}_{\mathrm{PLL}}]$ and the Metzler matrix

$$N := -[\widehat{\mathbf{v}}^{\mathrm{ref}}_{\mathrm{oq}}][\boldsymbol{\tau}'_{\mathrm{s}}]^{-1} + [\widehat{\mathbf{i}}^{\mathrm{ref}}_{\mathrm{oq}}]\widehat{L}^{-1}_{\mathrm{red}}[\boldsymbol{\tau}'_{\mathrm{s}}]^{-1} \tag{29}$$

is Hurwitz, then there exists $\epsilon^* > 0$ such that for every $\epsilon \leq \epsilon^*$, equilibrium $\widehat{\mathbf{x}}^{\mathrm{ref}}_0$ is locally exponentially stable.

Proof. Regarding part (i), since the network is resistive and power injections/demands are purely active, we know that

$$\widehat{Y}^{-1}_{\mathrm{red}} = \widehat{L}^{-1}_{\mathrm{red}} \otimes I_2, \quad \widehat{\mathbf{s}}^{\mathrm{ref}} = \widehat{\mathbf{p}}^{\mathrm{ref}} \otimes \left(\begin{smallmatrix} 1 \\ 0 \end{smallmatrix}\right) \quad \widehat{\mathbf{w}} = \widehat{\mathbf{u}} \otimes I_2.$$

Therefore: $\Big\|\mathcal{D}'(\widehat{\mathbf{w}})\widehat{Y}^{-1}_{\mathrm{red}}(\mathcal{D}'(\widehat{\mathbf{w}}))^{-1}\mathrm{D}'(\mathbf{s}^{\mathrm{ref}})\Big\|_{\mathbb{C},\infty} = \Big\|[\widehat{\mathbf{u}}]\widehat{L}^{-1}_{\mathrm{red}}[\widehat{\mathbf{u}}]^{-1}[\widehat{\mathbf{p}}^*]\Big\|_{\mathbb{C},\infty}$. The result then follows from Theorem 7(i). Regarding part (ii), since there are no reactive-power injections from the inverters, we have $\widehat{\mathbf{i}}^{\mathrm{ref}}_{\mathrm{od}} = \mathbb{0}_n$. Since the input voltage for the PLL and power controller is the *output* voltage of the LC filter (i.e., $\widehat{\mathbf{v}}^{\mathrm{ref}}_{\mathrm{odq}}$), and the network is purely resistive, we have $\widehat{\mathbf{v}}^{\mathrm{ref}}_{\mathrm{oD}} = \mathbb{0}_n$ and as a result $\boldsymbol{\delta}^{\mathrm{ref}} = \mathbb{0}_n$. Alternatively, this observation can be proved rigorously as follows. Since the power injections are purely active, the power injection vector $\mathbf{s}^{\mathrm{ref}}$ has the form $\mathbf{s}^{\mathrm{ref}} = \mathbf{p}^{\mathrm{ref}} \otimes \left(\begin{smallmatrix} 1 \\ 0 \end{smallmatrix}\right)$. Therefore, starting from the initial condition $\mathbf{v}^{(0)} = \widehat{\mathbf{w}} = \widehat{\mathbf{u}} \otimes \left(\begin{smallmatrix} 0 \\ 1 \end{smallmatrix}\right)$, the kth iteration in Lemma 16(ii) has the form $\mathbf{v}^{(k)} = \mathbf{u}^{(k)} \otimes \left(\begin{smallmatrix} 0 \\ 1 \end{smallmatrix}\right)$, for every integer $k \in \mathbb{Z}_{\geq 0}$. This implies that, in the limit, we have $\widehat{\mathbf{v}}^{\mathrm{ref}}_{\mathrm{oD}} = \mathbb{0}_n$ and as a result $\boldsymbol{\delta}^{\mathrm{ref}} = \mathbb{0}_n$. Therefore, the matrix M in condition (18) simplifies as shown below:

$$\begin{aligned} M &= -\Big([\widehat{\mathbf{v}}^{\mathrm{ref}}_{\mathrm{oq}}] \otimes I_2 - [\widehat{\mathbf{i}}^{\mathrm{ref}}_{\mathrm{oq}}]\widehat{L}^{-1}_{\mathrm{red}} \otimes I_2\Big)[\boldsymbol{\tau}'_{\mathrm{s}} \otimes I_2]^{-1} \\ &= -[\widehat{\mathbf{v}}^{\mathrm{ref}}_{\mathrm{oq}}][\boldsymbol{\tau}'_{\mathrm{s}}]^{-1} \otimes I_2 - [\widehat{\mathbf{i}}^{\mathrm{ref}}_{\mathrm{oq}}]\widehat{L}^{-1}_{\mathrm{red}}[\boldsymbol{\tau}'_{\mathrm{s}}]^{-1} \otimes I_2. \end{aligned}$$

Using Lemma 14, matrix M is Hurwitz if and only if matrices

$$-\big([\widehat{\mathbf{v}}^{\mathrm{ref}}_{\mathrm{oq}}] \pm [\widehat{\mathbf{i}}^{\mathrm{ref}}_{\mathrm{oq}}]\widehat{L}^{-1}_{\mathrm{red}}\big)[\boldsymbol{\tau}'_{\mathrm{s}}]^{-1} \tag{30}$$

are Hurwitz. Note that the active-power injections from the inverters to the grid are non-negative in steady state. This implies that $\widehat{\mathbf{i}}^{\mathrm{ref}}_{\mathrm{oq}} \geq \mathbb{0}_n$. Thus, the matrices (30) are similar to the following matrices:

$$-[\boldsymbol{\tau}'_{\mathrm{s}}]^{\frac{-1}{2}}[\widehat{\mathbf{v}}^{\mathrm{ref}}_{\mathrm{oq}}][\boldsymbol{\tau}'_{\mathrm{s}}]^{\frac{-1}{2}} \pm [\boldsymbol{\tau}'_{\mathrm{s}}]^{\frac{-1}{2}}[\widehat{\mathbf{i}}^{\mathrm{ref}}_{\mathrm{oq}}]^{\frac{1}{2}}\widehat{L}^{-1}_{\mathrm{red}}[\widehat{\mathbf{i}}^{\mathrm{ref}}_{\mathrm{oq}}]^{\frac{1}{2}}[\boldsymbol{\tau}'_{\mathrm{s}}]^{\frac{-1}{2}}.$$

Since the matrix $[\widehat{\mathbf{v}}^{\mathrm{ref}}_{\mathrm{oq}}]$ is positive definite and the matrix $[\widehat{\mathbf{i}}^{\mathrm{ref}}_{\mathrm{oq}}]^{\frac{1}{2}}\widehat{L}^{-1}_{\mathrm{red}}[\widehat{\mathbf{i}}^{\mathrm{ref}}_{\mathrm{oq}}]^{\frac{1}{2}}$ is positive semidefinite, the matrix

$$-[\boldsymbol{\tau}'_{\mathrm{s}}]^{\frac{-1}{2}}[\widehat{\mathbf{v}}^{\mathrm{ref}}_{\mathrm{oq}}][\boldsymbol{\tau}'_{\mathrm{s}}]^{\frac{1}{2}} - [\boldsymbol{\tau}'_{\mathrm{s}}]^{\frac{1}{2}}[\widehat{\mathbf{i}}^{\mathrm{ref}}_{\mathrm{oq}}]^{\frac{1}{2}}\widehat{L}^{-1}_{\mathrm{red}}[\widehat{\mathbf{i}}^{\mathrm{ref}}_{\mathrm{oq}}]^{\frac{1}{2}}[\boldsymbol{\tau}'_{\mathrm{s}}]^{\frac{-1}{2}}$$

is Hurwitz. Moreover, note that the matrix L_{red} is a grounded Laplacian matrix and by [5, Exercise 10.11] its inverse L^{-1}_{red} is non-negative. Also, the matrices $[\boldsymbol{\tau}'_{\mathrm{s}}]$, $[\widehat{\mathbf{i}}^{\mathrm{ref}}_{\mathrm{oq}}]$, and $[\widehat{\mathbf{v}}^{\mathrm{ref}}_{\mathrm{oq}}]$ are all diagonal with non-negative diagonal elements. This implies that the matrix $-[\widehat{\mathbf{v}}^{\mathrm{ref}}_{\mathrm{oq}}][\boldsymbol{\tau}'_{\mathrm{s}}]^{-1} + [\widehat{\mathbf{i}}^{\mathrm{ref}}_{\mathrm{oq}}]\widehat{L}^{-1}_{\mathrm{red}}[\boldsymbol{\tau}'_{\mathrm{s}}]^{-1}$ has non-negative off-diagonal elements and therefore, it is Metzler. The proof of Corollary (10) then follows from Theorem 7. □

2325-5870 (c) 2021 IEEE. Personal use is permitted, but republication/redistribution requires IEEE permission. See http://www.ieee.org/publications_standards/publications/rights/index.html for more information.
Authorized licensed use limited to: University of Washington Libraries. Downloaded on April 19,2022 at 20:42:08 UTC from IEEE Xplore. Restrictions apply.

This article has been accepted for publication in a future issue of this journal, but has not been fully edited. Content may change prior to final publication. Citation information: DOI 10.1109/TCNS.2021.3084444, IEEE Transactions on Control of Network Systems

Remark 11 (Computational complexity)**.** *One can check the Hurwitzness of the Metzler matrix* (29) *using the following feasibility problem:*

$$N\xi < 0, \quad \xi > 0. \tag{31}$$

The problem (31) *is a linear program and can be checked using distributed methods whose computational time scales linearly with the number of non-zero elements in* N *[21].*

V. Numerical Simulations

In this section, motivated by the recent increase in the integration of renewable energy resources across power grids, we study the stability issues associated with the expansion of networks of grid-following inverters. Our goal is to use Theorem 7 to study how the expansion of inverter networks can affect their small-signal stability. We present numerical simulation results for radial networks (see Fig. 2) with identical inverters and reference-power setpoints. Since Theorem 7 requires singular perturbation parameters $\epsilon_{\rm I}, \epsilon_{\mathcal{E}}$ to be small, we assume that $\epsilon_{\mathcal{E}}$ is small and fixed while $\epsilon_{\rm I}$ is small but variable. We aim to answer the following questions:[1]

- For which values of the inverter parameter $\epsilon_{\rm I}$ does Theorem 7(ii) guarantee small-signal stability?
- How efficient is the condition (18) in Theorem 7(ii) to analyze small-signal stability?

The first question can be interpreted as an *inverter design* problem, while the second question can be interpreted as a *network monitoring* problem. Solutions to these problems are provided in Sections V-A and V-B, respectively. Our test case is a family of radial networks $\{G(n)\}_{n\in\mathbb{N}}$, where $G(n)$ is the weighted undirected connected graph with the node set (buses) $\mathcal{N}_n = \{0,\dots,n\}$ and the edge set (branches) $\mathcal{E}_n = \{(i,i+1) \mid i = 0,\dots,n-1\}$ (see Fig. 2). For every radial network $G(n)$, the node 0 is the slack bus connected to the grid with voltage $v_{\rm g} = {\rm i}(120\sqrt{2})$ V(peak) and frequency $\omega_{\rm nom} = 120\pi$ rad/s. Nodes $\{1,\dots,n\}$ are the inverters with $s_{\rm nom} = 1000$ VA, and $\tau_{\rm PLL} = \epsilon_{\rm I}^2$, $\tau'_{\rm PLL} = \epsilon_{\rm I}^2 V_{\rm g}^{-1}$, ${\rm T}_{\rm PLL} = \epsilon_{\rm I}$, $\tau_{\rm s} = \epsilon_{\rm I}$, $\tau'_{\rm s} = (0.1)V_{\rm g}$, ${\rm T}_{\rm s} = 10\epsilon_{\rm I}$, $\tau_{\rm c} = \frac{V_{\rm g}}{s_{\rm nom}}\epsilon_{\rm I}^2$, ${\rm T}_{\rm c} = \epsilon_{\rm I}^2$, $L_{\rm f} = 10^{-3}$ H, and $C_{\rm f} = 2\times 10^{-3}$ F. For every $(j,k) \in \mathcal{E}_n$, the admittance of line (i,j) is given by $a_{jk} = a_{kj} = (RI_2 + \omega_{\rm nom} L\mathcal{J})^{-1}$, where the line resistance is $R = 0.02\ \Omega$ and line inductance is $L = 2\times 10^{-5}$ H. We first define the notion of a *safe penetration level*.

Definition 12 (Safe Penetration Level)**.** *Given a family of networks* $\{G(n)\}_{n\in\mathbb{N}}$ *and uniform reference power injection* $s^{\rm ref} \in \mathbb{R}^2$*, the Safe Penetration Level (SPL) for* $\{G(n)\}_{n\in\mathbb{N}}$ *is the maximum* $n \in \mathbb{N}$ *such that the dimensionless dynamics* (10) *with underlying graph* $G(n)$ *and reference powers* $\mathbf{s}^{\rm ref} = \mathbb{1}_n \otimes s^{\rm ref}$ *has a locally stable equilibrium point.*

Remark 13. *(1) For our test case network, SPL of the network depends on the parameter* $\epsilon_{\rm I}$*;*

(2) One can use the matrix M *defined in* (18) *to estimate the SPL of the network; from Theorem 7(ii), there exists* $\epsilon^* > 0$ *such that, for every* $\epsilon \le \epsilon^*$*, SPL of the network is larger than this estimate.*

[1]All the numerical simulations are performed in MATLAB R2016a on a computer with Intel Core i5 processor @ 1.6 GHZ CPU and 4 GB RAM.

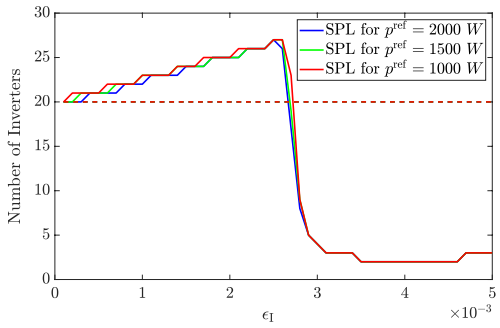

Fig. 4: SPL for different active power injections. Dashed lines show estimates of SPL computed using Hurwitzness of matrix M.

A. Designing Grid-tied Inverter Networks

We now examine the efficiency of our analytic results in Theorem 7 to design grid-following inverter networks focusing on the small-signal stability of the grid. In particular, we focus on estimating the SPL for the radial network shown in Fig 2 and numerically computing the largest range of parameter $\epsilon_{\rm I}$ for which Theorem 7(ii) holds. To carry out this task, we study the effect of parameter $\epsilon_{\rm I}$ for different active power injections on the SPL of the system. The result is shown in Fig. 4, where the overlapping dashed lines are the estimates of SPL based on the sufficient condition in Theorem 7(ii). Thus, according to Fig. 4, the largest domain $\epsilon_{\rm I}$ for which Theorem 7(ii) holds is $(0, 0.0025]$, for the active power injections $p^{\rm ref} = 1000\ W$, $p^{\rm ref} = 1500\ W$, and $p^{\rm ref} = 2000\ W$, respectively. As $\epsilon_{\rm I}$ becomes smaller, the dashed and solid lines get closer to each other and Theorem 7(ii) can be used to find the exact SPL.

B. Monitoring Grid-tied Inverter Networks

We now study the accuracy and computational efficiency of condition (18) in Theorem 7(ii) for monitoring the small-signal stability of the network. For our test case, we pick the parameter $\epsilon_{\rm I} = 0.001$. Based on the discussion in Section V-A, we are in the range of applicability of Theorem 7(ii). Recall that SPL is the largest number of inverters in the network for which the equilibrium point $\widehat{\mathbf{x}}_0^{\rm ref}$ of full-order system (10) is locally asymptotically stable. We let ${\rm T}_{\rm lin}$ denote the computational time of finding SPL, using the eigenvalue analysis for the linearized system. We let ${\rm SPL}_{\rm test}$ denote the largest number of inverters in the grid for which the matrix M in (18) is Hurwitz. Similarly, we let ${\rm T}_{\rm test}$ denote the computational time for checking the Hurwitzness of matrix M in (18). Finally, we let ${\rm SPL}_{\rm static}$ denote the largest number of inverters in the grid for which condition (15) holds. We start with different uniform reference active-power injections $\widehat{\rm s}^{\rm ref} = \mathbb{1}_n \otimes (\widehat{p}, 0)^\top$ and compute the thresholds SPL, ${\rm SPL}_{\rm test}$, and ${\rm SPL}_{\rm static}$ together with the computational times for SPL and ${\rm SPL}_{\rm test}$, for each active-power injections. The results are shown in Table I. From Table I, one can see that (i) the static condition (15) overestimates the value of SPL, (ii) condition (18) gives an accurate lower bound for safe penetration level and its

2325-5870 (c) 2021 IEEE. Personal use is permitted, but republication/redistribution requires IEEE permission. See http://www.ieee.org/publications_standards/publications/rights/index.html for more information.
Authorized licensed use limited to: University of Washington Libraries. Downloaded on April 19,2022 at 20:42:08 UTC from IEEE Xplore. Restrictions apply.

This article has been accepted for publication in a future issue of this journal, but has not been fully edited. Content may change prior to final publication. Citation information: DOI 10.1109/TCNS.2021.3084444, IEEE Transactions on Control of Network Systems

corresponding computation time (i.e., $\mathrm{T_{test}}$) is almost one order of magnitude less that the computation time to perform eigenvalue analysis for the full-order system (i.e., $\mathrm{T_{lin}}$).

$\widehat{p}$	$\mathrm{T_{lin}}$ (s)	$\mathrm{T_{test}}$ (s)	SPL	$\mathrm{SPL_{test}}$	$\mathrm{SPL_{static}}$
0.80	0.5853	0.0774	22	20	35
1.00	0.5636	0.0793	22	20	31
1.20	0.5546	0.0741	22	20	28
1.40	0.6525	0.0767	22	20	26
1.60	0.5313	0.0767	21	20	24
1.80	0.5063	0.0888	21	20	23
2.00	0.5241	0.0766	21	20	22

TABLE I: Comparing the computation time and accuracy of conditions (18) and (15) for small-signal stability. The unit of the quantities $\mathrm{T_{test}}$ and $\mathrm{T_{lin}}$ are seconds, the quantity of $\widehat{p}$ is dimensionless and the quantities SPL and $\mathrm{SPL_{test}}$ and $\mathrm{SPL_{static}}$ are integers.

VI. Conclusions & Future Work

We studied small-signal stability of grid-tied networks of grid-following inverters and loads. Using a time-scale analysis and a suitable choice of a family of parameters for the inverters, we presented an analytic sufficient condition for local exponential stability. We showed that, compared to the direct eigenvalue analysis of the full-order system, this sufficient condition has the advantages of reducing the computational complexity of checking small-signal stability as well as providing insights about the role of the network topology and inverter parameters on stability. Directions for future work include expanding the scope of the analytical approach to include other inverter control methods, DC-side dynamics, and load models. Expansive case studies focused on standard IEEE test cases with deliberately introduced heterogeneity in network and inverter parameters would also highlight the benefits of the proposed analytical approach to practitioners and operators engaged in system design and monitoring.

Appendix

Table (II) collects the variables and their symbols for grid-following inverter model and Table (III) collects the parameter values for this class of inverters.

Variable	Symbol	Variable	Symbol
PLL low-pass filter state	v_{PLL}	Current controller auxiliary state	γ_{dq}
PLL PI controller state	ϕ_{PLL}	Current controller output voltage	v_{idq}
PLL phase output	δ	Output current	i_{odq}
Power controller low-pass filter state	s_{ave}	Power controller auxiliary state	ϕ_{s}
Reference power injection	s^{ref}	Current controller reference current	i_{Idq}
Power controller auxiliary state	ϕ_{s}	PLL Frequency	ω_{PLL}
Current in the lines	ξ_{DQ}	LC-filter voltage	v_{odq}
Grid voltage	v_{gDQ}	Grid frequency	ω_{nom}

TABLE II: Variables and their symbols for the inverter model.

Lemma 14. *Let $\eta_1, \ldots, \eta_m$ be the eigenvalues of a matrix $C \in \mathbb{C}^{m\times m}$. For $A, B \in \mathbb{C}^{n\times n}$, λ is an eigenvalue of $A \otimes I_m + B \otimes C$ if and only if it is an eigenvalue of $A + \eta_k B$, for some $k \in \{1, \ldots, m\}$.*

Parameter	Symbol	Values from [23]	Values from [17]
Grid frequency	ω_{nom}	377 rad/s	377 rad/s
Grid voltage amplitude	V_{g}	169 V	169 V
PLL time constant	τ_{PLL}	1.27e−5	1.27e−5
PLL time constant	τ'_{PLL}	2.36e−2	4.7e−3
PLL time constant	T_{PLL}	1.25e−1	1.25e−1
Power controller time constant	τ_{s}	1.99e−2	1.99e−2
Power controller time constant	τ'_{s}	16.97	16.97
Power controller time constant	T_{s}	1.00e−1	1.00e−1
Current controller time constant	τ_{c}	1.70e−3	7.85e−4
Current controller time constant	T_{c}	1.00e−2	1.43e−3
LC time constant	τ_{LC}	2.37e−5	2.54e−5
LC time constant	τ'_{LC}	2.37e−5	2.54e−5
Line time constant	τ_{e}	1.90e−3	2.70e−3
Line time constant	τ'_{e}	7.40e−3	1.31e−0

TABLE III: Dimensionless parameters of the inverter model.

Lemma 15. *Let $\Gamma, \Pi, \Xi, \Upsilon, \Sigma, \in \mathbb{R}^{n\times n}$ and $\Theta \in \mathbb{R}^{m\times m}$ be diagonal matrices with positive diagonal entries such that $\Gamma \succ \Sigma$. Suppose that $K \in \mathbb{R}^{m\times n}$ is an arbitrary matrix with $\mathrm{Ker}(K) = \{\mathbb{0}_n\}$, $P \in \mathbb{R}^{n\times n}$ is a skew-symmetric matrix, and $Z \in \mathbb{R}^{m\times m}$ is such that $Z + Z^\top$ is negative definite. Then the following matrices are Hurwitz:*

$$A = \begin{pmatrix} -\Gamma & \mathbb{0}_{n\times n} & \Upsilon \\ -\Sigma & \mathbb{0}_{n\times n} & \mathbb{0}_{n\times n} \\ -\Xi & \Xi & \mathbb{0}_{n\times n} \end{pmatrix}, B = \begin{pmatrix} \mathbb{0}_{n\times n} & -\Gamma & \mathbb{0}_{n\times n} & \mathbb{0}_{n\times m} \\ \Xi & -\Upsilon & -\Xi & \mathbb{0}_{n\times m} \\ \mathbb{0}_{n\times n} & \Pi & \Pi P & -\Pi K^\top \\ \mathbb{0}_{m\times n} & \mathbb{0}_{m\times n} & \Theta K & \Theta Z \end{pmatrix}.$$

Proof. The characteristic polynomial of matrix A is: $\lambda^3 I_n + \lambda^2\Gamma + \lambda\Upsilon\Xi + \Upsilon\Xi\Sigma = \mathbb{0}_n$. Since all matrices Γ, Σ, Ξ, and Υ are diagonal, λ_i is an eigenvalue of A if and only if $\lambda_i^3 I_n + \lambda_i^2(\Gamma)_i + \lambda_i(\Upsilon)_i(\Xi)_i + (\Upsilon)_i(\Xi)_i(\Sigma)_i = 0$. The diagonal elements of the matrices Γ, Σ, Ξ, and Υ are positive. Therefore, using the Routh–Hurwitz criteria, $\lambda_i \in \mathbb{C}_-$ if and only if $(\Gamma)_i(\Upsilon)_i(\Xi)_i > (\Sigma)_i(\Upsilon)_i(\Xi)_i$. Thus, A is Hurwitz if and only if $\Gamma \succ \Sigma$. To show that the matrix B is Hurwitz, we use LaSalle's invariance principle [11, Theorem 4.4]. Consider the dynamical system $\dot{\mathrm{x}} = B\mathrm{x}$, where $\mathrm{x} = (\mathrm{x}_1, \mathrm{x}_2, \mathrm{x}_3, \mathrm{x}_4)^\top \in \mathbb{R}^{(6n+m)}$. We define the Lyapunov function $V : \mathbb{R}^{(6n+m)} \to \mathbb{R}$ by: $V(\mathrm{x}_1, \mathrm{x}_2, \mathrm{x}_3, \mathrm{x}_4) = \frac{1}{2}\big(\mathrm{x}_1^\top\Gamma^{-1}\mathrm{x}_1 + \mathrm{x}_2^\top\Xi^{-1}\mathrm{x}_2 + \mathrm{x}_3^\top\Pi^{-1}\mathrm{x}_3 + \mathrm{x}_4^\top\Theta^{-1}\mathrm{x}_4\big)$ Then, it is easy to check that $\dot{V}(\mathrm{x}_1, \mathrm{x}_2, \mathrm{x}_3) = -\mathrm{x}_2^\top\Upsilon\Xi^{-1}\mathrm{x}_2 + \frac{1}{2}\mathrm{x}_4^\top(Z + Z^\top)\mathrm{x}_4$. Therefore, by LaSalle's invariance principle, the trajectories of the system $\dot{\mathrm{x}} = B\mathrm{x}$ converges to the largest invariant set inside $S = \{\mathrm{x} \in \mathbb{R}^{(6n+m)} \mid \dot{V}(\mathrm{x}) = 0\}$. It is easy to see that $S = \{\mathrm{x} \in \mathbb{R}^{6n} \mid \mathrm{x}_4 = \mathrm{x}_2 = \mathbb{0}_n\}$. Let us denote the largest invariant set inside S by L. Our goal is to show that $L = \{\mathbb{0}_{(6n+m)}\}$. Suppose that $\gamma : t \mapsto (\gamma_1(t), \gamma_2(t), \gamma_3(t), \gamma_4(t))$ is a trajectory which belongs identically to S. Then we have $\gamma_4(t) = \gamma_2(t) = \mathbb{0}_n$. First note that $\dot{\gamma}_4(t) = 0$ implies that $\Theta K\gamma_3(t) + \Theta Z\gamma_4(t) = \Theta K\gamma_3(t) = \mathbb{0}_m$. Since $\mathrm{Ker}(K) = \{\mathbb{0}_m\}$, we deduce that $\gamma_3(t) = 0$. Moreover, we see that $\dot{\gamma}_2(t) = \mathbb{0}_n \implies \Xi\gamma_1(t) = \mathbb{0}_n$. This implies that $\gamma_1(t) = \gamma_2(t) = \gamma_3(t) = \gamma_4(t) = 0$. Thus, the only invariant set inside S is $\{\mathbb{0}_{(6n+m)}\}$ and thus B is Hurwitz. □

Lemma 16. *Consider (12), (13) with $\widehat{\mathbf{w}} = -\widehat{Y}_{\mathrm{red}}^{-1}\widehat{Y}_{0\mathrm{g}}$. Suppose $\|\mathcal{D}'(\widehat{\mathbf{w}})\widehat{Y}_{\mathrm{red}}^{-1}(\mathcal{D}'(\widehat{\mathbf{w}}))^{-1}\mathcal{D}'(\widehat{\mathbf{s}}^*)\|_{\mathbb{C},\infty} \leq \frac{3}{8}$. Then, the following statements hold:*

(i) the power flow equations (12) and (13) has a unique solution $(\widehat{\mathbf{v}}^*_{\mathrm{oDQ}}, \widehat{\mathbf{i}}^*_{\mathrm{oDQ}})$ with $\widehat{\mathbf{v}}^*_{\mathrm{oDQ}} \in \Omega$, where $\Omega = \big\{\mathbf{y} \in \mathbb{R}^{2n} \mid \|\mathbf{y} - \widehat{\mathbf{w}}\|_{\mathbb{C},\infty} \leq \frac{1}{2}\|\widehat{\mathbf{w}}\|_{\mathbb{C},\infty}\big\}$;

2325-5870 (c) 2021 IEEE. Personal use is permitted, but republication/redistribution requires IEEE permission. See http://www.ieee.org/publications_standards/publications/rights/index.html for more information.
Authorized licensed use limited to: University of Washington Libraries. Downloaded on April 19,2022 at 20:42:08 UTC from IEEE Xplore. Restrictions apply.

This article has been accepted for publication in a future issue of this journal, but has not been fully edited. Content may change prior to final publication. Citation information: DOI 10.1109/TCNS.2021.3084444, IEEE Transactions on Control of Network Systems

(ii) for every $\mathbf{v}^0 \in \Omega$*, the iteration procedure*

$$\mathbf{v}^{k+1} = \widehat{\mathbf{w}} + \tfrac{2}{3}\widehat{Y}_{\text{red}}^{-1}\mathcal{D}(\mathbf{v}^k)^{-1}\widehat{\mathbf{s}}^*, \qquad \forall k \in \mathbb{N},$$

converges to $\widehat{\mathbf{v}}^*_{\text{oDQ}}$*, where* $(\widehat{\mathbf{v}}^*_{\text{oDQ}}, \widehat{Y}_{\text{red}}(\widehat{\mathbf{v}}^*_{\text{oDQ}} - \widehat{\mathbf{w}}))$ *is the unique solution to* (12) *and* (13)*.*

Proof. By considering $\mathbb{R}^{2n} \simeq \mathbb{C}^n$, part (i) and (ii) are straightforward generalizations of [30, Theorem 1]. One should note the fact that the nodal variables in [30, Theorem 1] are average power injections/demands and therefore the power flow equations have the form $S = V\overline{I}$. However, in this paper, the nodal variables are instantaneous power injections/demands and the power flow equations read $s = \frac{3}{2}\mathcal{D}(v_{\text{odq}})i_{\text{odq}}$. □

REFERENCES

[1] J. L. Agorreta, M. Borrega, J. López, and L. Marroyo. Modeling and control of N-paralleledx grid-connected inverters with LCL filter coupled due to grid impedance in PV plants. *IEEE Transactions on Power Electronics*, 26(3):770–785, 2011.

[2] O. Ajala, A. D. Domínguez-García, and P. W. Sauer. *A Hierarchy of Models for Inverter-Based Microgrids*, pages 307–332. Springer, 2018.

[3] H. Akagi, E. H. Watanabe, and M. Aredes. *Instantaneous Power Theory and Applications to Power Conditioning*. John Wiley & Sons, 2017.

[4] S. Bolognani and S. Zampieri. On the existence and linear approximation of the power flow solution in power distribution networks. *IEEE Transactions on Power Systems*, 31(1):163–172, 2016.

[5] F. Bullo. *Lectures on Network Systems*. Kindle Direct Publishing, 1.4 edition, 2020.

[6] S. Curi, D. Groß, and F. Dörfler. Control of low inertia power grids: A model reduction approach. In *IEEE Conf. on Decision and Control*, pages 5708–5713, 2017.

[7] F. Dörfler and F. Bullo. Kron reduction of graphs with applications to electrical networks. *IEEE Transactions on Circuits and Systems I: Regular Papers*, 60(1):150–163, 2013.

[8] P. Fairley. 800,000 Microinverters Remotely Retrofitted on Oahu—in One Day. *IEEE Spectrum*, 5 Feb 2015.

[9] D. Groß, C. Arghir, and F. Dörfler. On the steady-state behavior of a nonlinear power system model. *Automatica*, 90:248–254, 2018.

[10] R. A. Horn and C. R. Johnson. *Matrix Analysis*. Cambridge University Press, 2012.

[11] H. K. Khalil. *Nonlinear Systems*. Prentice Hall, 3 edition, 2002.

[12] P. V. Kokotović, H. K. Khalil, and J. O'Reilly. *Singular Perturbation Methods in Control: Analysis and Design*. SIAM, 1999.

[13] Y. Lin, B. Johnson, V. Gevorgian, V. Purba, and S. Dhople. Stability assessment of a system comprising a single machine and inverter with scalable ratings. In *North American Power Symposium*, pages 1–6, 2017.

[14] L. Luo and S. V. Dhople. Spatiotemporal model reduction of inverter-based islanded microgrids. *IEEE Transactions on Energy Conversion*, 29(4):823–832, 2014.

[15] U. Markovic, O. Stanojev, E. Vrettos, P. Aristidou, and G. Hug. Understanding stability of low-inertia systems. *engrXiv*, 2019.

[16] C. A. Plet, M. Graovac, T. C. Green, and R. Iravani. Fault response of grid-connected inverter dominated networks. In *IEEE PES General Meeting*, pages 1–8, 2010.

[17] N. Pogaku, M. Prodanovic, and T. C. Green. Modeling, analysis and testing of autonomous operation of an inverter-based microgrid. *IEEE Transactions on Power Electronics*, 22(2):613–625, 2007.

[18] M. Prodanovic and T. C. Green. Control and filter design of three-phase inverters for high power quality grid connection. *IEEE Transactions on Power Electronics*, 18(1):373–380, 2003.

[19] V. Purba, S. Jafarpour, B. B. Johnson, F. Bullo, and S. V. Dhople. Reduced-order structure-preserving model for parallel-connected three-phase grid-tied inverters. In *IEEE Workshop on Control and Modeling for Power Electronics*, 2017.

[20] V. Purba, B. B. Johnson, S. Jafarpour, F. Bullo, and S. V. Dhople. Dynamic aggregation of grid-tied three-phase inverters. *IEEE Transactions on Power Systems*, 35(2):1520–1530, 2020.

[21] A. Rantzer. Scalable control of positive systems. *European Journal of Control*, 24:72–80, 2015.

[22] M. Rasheduzzaman, J. A. Mueller, and J. W. Kimball. An accurate small-signal model of inverter-dominated islanded microgrids using *dq* reference frame. *IEEE Journal of Emerging and Selected Topics in Power Electronics*, 2(4):1070–1080, 2014.

[23] M. Rasheduzzaman, J. A. Mueller, and J. W. Kimball. Reduced-order small-signal model of microgrid systems. *IEEE Transactions on Sustainable Energy*, 6(4):1292–1305, 2015.

[24] V. R. Saksena, J. O'Reilly, and P. V. Kokotovíc. Singular perturbations and time-scale methods in control theory: Survey 1976-1983. *Automatica*, 20(3):273–293, 1984.

[25] J. Schiffer, D. Zonetti, R. Ortega, A. M. Stanković, T. Sezi, and J. Raisch. A survey on modeling of microgrids — From fundamental physics to phasors and voltage sources. *Automatica*, 74:135–150, 2016.

[26] I. Subotic, D. Gross, M. Colombino, and F. Dörfler. A Lyapunov framework for nested dynamical systems on multiple time scales with application to converter-based power systems. *IEEE Transactions on Automatic Control*, 2020. in press.

[27] E. Twining and D. G. Holmes. Grid current regulation of a three-phase voltage source inverter with an LCL input filter. *IEEE Transactions on Power Electronics*, 18(3):888–895, 2003.

[28] D. Venkatramanan and V. John. Dynamic phasor modeling and stability analysis of SRF-PLL-based grid-tie inverter under islanded conditions. *IEEE Transactions on Industry Applications*, 56(2):1953–1965, 2020.

[29] P. Vorobev, P. H. Huang, M. Al Hosani, J. L. Kirtley, and K. Turitsyn. High-fidelity model order reduction for microgrids stability assessment. *IEEE Transactions on Power Systems*, 33(1), 2017.

[30] C. Wang, A. Bernstein, J. Y. Le Boudec, and M. Paolone. Explicit conditions on existence and uniqueness of load-flow solutions in distribution networks. *IEEE Transactions on Smart Grid*, 9(2):953–962, 2018.

[31] A. Yazdani and R. Iravani. *Voltage-Sourced Converters in Power Systems: Modeling, Control, and Applications*. IEEE Press, 2010.

[32] C. Yu, X. Zhang, F. Liu, F. Li, H. Xu, R. Cao, and H. Ni. Modeling and resonance analysis of multiparallel inverters system under asynchronous carriers conditions. *IEEE Transactions on Power Electronics*, 32(4):3192–3205, 2017.

Saber Jafarpour (M'16) is a Postdoctoral researcher with the Mechanical Engineering Department and the Center for Control, Dynamical Systems and Computation at the University of California, Santa Barbara. He received his Ph.D. in 2016 from the Department of Mathematics and Statistics at Queen's University. His research interests include analysis of network systems with application to power grids and geometric control theory.

Victor Purba (S'15) received the bachelor's and M.S. degrees in electrical engineering in 2014 and 2016, respectively, from the University of Minnesota, Minneapolis, MN, USA, where he is currently working toward the Ph.D. degree in electrical engineering. His research interests include modeling, analysis, and control of power systems with the integration of renewable energy sources.

Brian Johnson (S'08–M'13) received the M.S. and Ph.D. degrees in electrical and computer engineering from the University of Illinois at Urbana-Champaign, Champaign, IL, USA, in 2010 and 2013, respectively. He is an Assistant Professor with the Department of Electrical Engineering, University of Washington, Seattle, WA, USA. Prior to joining the faculty with the University of Washington in 2018, he was an Electrical Engineer with National Renewable Energy Laboratory, Golden, CO, USA. He was awarded a National Science Foundation Graduate Research Fellowship in 2010, and currently an Associate Editor for the IEEE TRANSACTIONS ON ENERGY CONVERSION. His research interests are in renewable energy systems, power electronics, and control systems.

Sairaj V. Dhople (M'13) received the B.S., M.S., and Ph.D. degrees in electrical engineering from the University of Illinois at Urbana-Champaign, Urbana, IL, USA, in 2007, 2009, and 2012, respectively. He is currently an Associate Professor with the Department of Electrical and Computer Engineering, University of Minnesota, Minneapolis, MN, USA. His research interests include modeling, analysis, and control of power electronics and power systems with a focus on renewable integration. He was the recipient of the National Science Foundation CAREER Award in 2015 and the Outstanding Young Engineer Award from the IEEE Power and Energy Society in 2019. He is an Associate Editor for the IEEE TRANSACTIONS ON ENERGY CONVERSION and the IEEE TRANSACTIONS ON POWER SYSTEMS.

Francesco Bullo (S'95-M'99-SM'03-F'10) is a Professor with the Mechanical Engineering Department and the Center for Control, Dynamical Systems and Computation at the University of California, Santa Barbara. His research interests focus on network systems and distributed control with application to robotic coordination, power grids and social networks. He is the coauthor of "Geometric Control of Mechanical Systems" (Springer, 2004), "Distributed Control of Robotic Networks" (Princeton, 2009), and "Lectures on Network Systems" (KDP, 2020, v1.4). He is a Fellow of IEEE, IFAC, and SIAM.

2325-5870 (c) 2021 IEEE. Personal use is permitted, but republication/redistribution requires IEEE permission. See http://www.ieee.org/publications_standards/publications/rights/index.html for more information.
Authorized licensed use limited to: University of Washington Libraries. Downloaded on April 19,2022 at 20:42:08 UTC from IEEE Xplore. Restrictions apply.